isvr Institute of Sound and Vibration Research

Studies into the Detection of Buried Objects (Particularly Optical Fibres) in Saturated Sediment. Part 4: Experimental Investigations into the Acoustic Detection of Objects Buried in Saturated Sediment

R.C.P. Evans and T.G. Leighton

ISVR Technical Report No 312

April 2007

University of Southampton

SCIENTIFIC PUBLICATIONS BY THE ISVR

Technical Reports are published to promote timely dissemination of research results by ISVR personnel. This medium permits more detailed presentation than is usually acceptable for scientific journals. Responsibility for both the content and any opinions expressed rests entirely with the author(s).

Technical Memoranda are produced to enable the early or preliminary release of information by ISVR personnel where such release is deemed to the appropriate. Information contained in these memoranda may be incomplete, or form part of a continuing programme; this should be borne in mind when using or quoting from these documents.

Contract Reports are produced to record the results of scientific work carried out for sponsors, under contract. The ISVR treats these reports as confidential to sponsors and does not make them available for general circulation. Individual sponsors may, however, authorize subsequent release of the material.

Studies into the detection of buried objects (particularly optical fibres) in saturated sediment. Part 4: Experimental investigations into the acoustic detection of objects buried in saturated sediment

R C P Evans and T G Leighton

ISVR Technical Report No. 312

April 2007

UNIVERSITY OF SOUTHAMPTON

INSTITUTE OF SOUND AND VIBRATION RESEARCH

FLUID DYNAMICS AND ACOUSTICS GROUP

Studies into the detection of buried objects (particularly optical fibres) in saturated sediment. Part 4: Experimental investigations into the acoustic detection of objects buried in saturated sediment

by

R C P Evans and T G Leighton

ISVR Technical Report No. 312

April 2007

Authorized for issue by
Professor R J Astley, Group Chairman

ACKNOWLEDGEMENTS

TGL is grateful to the Engineering and Physical Sciences Research Council and Cable & Wireless for providing a studentship for RCPE to conduct this project.

CONTENTS

FIGURE CAPTIONS

ABSTRACT

This report is the fourth in a series of five, designed to investigate the detection of targets buried in saturated sediment, primarily through acoustical or acoustics-related methods. Although steel targets are included for comparison, the major interest is in targets (polyethylene cylinders and optical fibres) which have a poor acoustic impedance mismatch with the host sediment. This particular report aims to review the signal processing requirements of the system and to investigate the relative performance of a number of different detection algorithms.

In order to do this, some basic signal processing concepts are presented and a number of different approaches to detection processing were discussed, noting that the detection system should be optimised to the class of object being sought. To this end, the scattering characteristics of spheres and cylinders are calculated. These were used to aid in the selection of an optimal frequency range for later incorporation into the detection algorithms.

The study examines the use of waveform dependent filtering, processing in a number of ways (forms of optimal filter and Synthetic Aperture Sonar, SAS) the same scattered data obtained with incident FM pulse compression waveforms. (There is a preliminary study which examines a simple scattered power measurement, using pulsed AM waveforms, but this can only be seen as rudimentary preparatory work because: (i) it cannot be compared with the waveform dependent filtering methods because it uses a different incident waveform; and (ii) the designers of a realistic system would almost certainly consider some form of matched filter, at the very least an attempt would be made to match the filter input bandwidth to that of the signal).

The algorithms presented in this report are applied in an experiment and prove to be very successful in detecting objects buried at depths of between 25 and 30 cm in the saturated sediment of the test tank. In every case, either 60 or 300 sample points were measured over a series of planes extending vertically into the sediment. It was found that with 60 points (having a sample spacing of 5 cm) the resolution was not high enough to provide conclusive detection results. Conversely, with 300 points (having a sample spacing of around 2 cm) the buried objects could readily be detected.

Simple matched filtering is shown to be useful in an environment dominated by noise. However, the optimal filter is shown to be more successful in dealing with the cluttered seabed environment. Target optimisation techniques had mixed success. When the target scattering responses (for both rigid and the elastic scattering) were incorporated into the filters, qualitative improvements in target localisation were observed. However, these were not accompanied by an increase in the average values of the signal-to-noise ratio.

The investigation into Synthetic Aperture techniques was limited by the positional error in the laboratory apparatus and the small number of measurement positions used to form the synthetic aperture. As a result of these experimental limitations, no significant performance improvement was actually observed.

This series of reports is written in support of the article "The detection by sonar of difficult targets (including centimetre-scale plastic objects and optical fibres) buried in saturated sediment" by T G Leighton and R C P Evans, written for a Special Issue of *Applied Acoustics* which contains articles on the topic of the detection of objects buried in marine sediment. Further support material can be found at http://www.isvr.soton.ac.uk/FDAG/uaua/target_in_sand.HTM.

LIST OF SYMBOLS

a_c	Radius of a cylindrical object
a_s	Radius of a spherical object
a_t	Radius of a target object
a(t)	Envelope function
$A_{\Omega\Xi}$	The element ΩΞ of a determinant, $D_n^{(\ldots)}$
c_L	Speed of sound in the direction of longitudinal waves
c_s	Speed of sound in sediment
c_T	Speed of sound in the direction of transverse waves
c_w	Speed of sound in water
CFAR	Constant false alarm rate
$D_n^{(\ldots)}$	Determinant
e	Exponential constant (2.71828182)
f	Frequency (Hz)
f_0	Carrier frequency
F_n	A quantity related to modal mechanical impedance
$F_R(\ldots)$	Frequency resolution constant
$f_\infty(\theta_s)$	The far-field form function
g(t)	Filter output signal in the absence of noise
h(t)	Matched filter impulse response function
$h_c(t)$	a continuous function
$h_n^{(1)}(\ldots)$	Spherical Hankel function of the first kind
$H_n^{(1)}(\ldots)$	Hankel function of the first kind
$H_c(f)$	The frequency domain representation of $h_c(t)$
$H(\omega)$	Frequency-domain transfer function

$H(\omega)$	The frequency-domain transfer function of the filter which optimises the signal-to-noise ratio
j	Complex operator, $\sqrt{-1}$
$j_n(\ldots)$	Spherical Bessel function of the first kind
$J_n(\ldots)$	Bessel function of the first kind
k	Wave number modulus
$\mathbf{k}$	Complex wave number
K_c	Clutter level
k_L	Wave number in the direction of longitudinal waves
k_n	A normalisation constant
k_T	Wave number in the direction of transverse waves
l	Length
l_1	Distance along ray from transmitter to interface
l_2	Distance along ray from point of interest in sediment to interface
N_0	One-sided noise power spectral density
n_n	Spherical Neumann function
$N(\omega)$	Noise signal
p_0	Acoustic pressure amplitude (zero-to-peak) of incident wave
P_n	The Legendre polynomials
P_N	Normalised noise power
p_{sc}	Scattered acoustic pressure
$P(f)$	The one-sided power spectral density
PRF	Pulse repetition frequency
$q_1(t)$	a generic function of time
$q_2(t)$	a generic function of time

$Q_1(\omega)$	the fourier transform of $q_1(t)$
$Q_2(\omega)$	the fourier transform of $q_2(t)$
Q	A general co-ordinate point
$Q(\omega)$	Measured signal (including noise)
r	Radial distance to the point of interest from a scattering centre
r_n	A function required to describe the far-field form function for scattering from a sphere
R_0	The range of a target at time $t = 0$
$R_n(\ldots)$	A function required to describe the far-field form function for scattering from a cylinder
R_{Pa}	Pressure amplitude reflection coefficient
R(t)	Range of a target as a function of time
$R(\omega)$	Transducer response function
S_0	Separation between acoustic elements or between an acoustic element and the back of a spherical reflector (point O)
s(t)	Signal input to the signal processor (excluding noise)
$s_{real}(t)$	A real waveform which corresponds to a driving signal
SAR	Synthetic aperture radar
SAS	Synthetic aperture sonar
SNR	Signal-to-noise ratio
SNR_{max}	The maximum signal-to-noise ratio
$S(\omega)$	Signal input to a signal processor (excluding noise)
t	Time
t_d	Variable delay time
T_d	Constant delay time
TOF	Time-of-flight of acoustic pulse
$T_R(\ldots)$	Time resolution constant
T_w	Half the duration of the time window

$u(t)$	A complex waveform representation of $s_{real}(t)$
$U(\omega)$	Signal output from a signal generator
$\tilde{U}(\omega)$	Output of an optimal filter in the presence of noise
v	Velocity
x	Cartesian co-ordinate in the horizontal plane
x_1	Co-ordinate value on x axis for point of interest in sediment
x_{Rx}	Horizontal co-ordinate position of Rx
x_{Tx}	Horizontal co-ordinate position of Tx
$X(\omega)$	Frequency response of a detection system
y	Cartesian co-ordinate in the horizontal plane
z	Cartesian co-ordinate in the vertical plane, and the axial position relative to the end of an optic fibre
Z	Characteristic acoustic impedance
z_B	Mean height of the water-sediment boundary
z_0	Co-ordinate value on z axis for transmisster and for receiver
z_1	Co-ordinate value on z axis for point of interest in sediment
α_s	Structure factor
$\chi(\tau, \phi)$	Complex time / frequency response function
Δ	Directivity function
δ_n	A term in the scattering function of a sphere
ε_n	Neumann factor ($\varepsilon_n = 1$ for $n = 0$, $\varepsilon_n = 2$ for $n > 0$)
ϕ	Frequency delay

ϕ_{rad}	Phase delay
$\Phi(\omega)$	Optimal filter
λ	Wavelength
λ_0	Correlation length
υ	Poisson's ratio
π	Pi (≈ 3.141592654)
θ_c	Critical angle
θ_i	Angle of incidence
θ_s	Scattering angle
θ_t	Angle of transmission
$\theta(t)$	Phase modulation
ρ_c	Density of a cylinder
ρ_f	Density of a fluid
ρ_s	Density of a sphere
σ_B	Back-scatter cross-section
σ_R	Rayleigh back-scattering cross-section
τ	Time delay variable
τ_{Pa}	Tensile strength
τ_r	Relaxation time
τ_w	Pulse width
ω	Circular frequency
ω_0	Natural circular frequency
ω_a	Acoustic wave circular frequency

ψ_i	Incident acoustic field
Ψ_I	Intrinsic signal-to-noise ratio
ψ_r	Reflected scalar wave potential
ψ_s	Scattered acoustic field
ψ_t	Transmitted scalar wave potential
$\psi(t)$	A complex time domain waveform, the real part of which is the driving signal $s_{real}(t)$
$\Psi(\omega)$	The complex frequency-domain representation of $\psi(t)$
∇	Differential operator $\left(\frac{\partial}{\partial x}, \frac{\partial}{\partial y}, \frac{\partial}{\partial z}\right)$

1 Introduction

This is the fourth report of a series of five. In the first report[1] in this series, acoustic systems were identified as having the greatest potential to detect difficult objects buried in the seabed. A laboratory test facility was described in the second report[2]. This comprised a water-filled tank, part-filled with sediment, a pair of focused transducers, and a computerised control system. The third report[3] addressed some issues that are important to the success of an acoustic detection system. It was important to deal with these before undertaking any detection experiments. In particular, it was noted that surface roughness can give rise to an increase in scatter within the sediment, especially at high grazing angles.

In this report, experiments involving the detection of real objects are presented. Emphasis is placed on the signal processing components of the system. Given the observations made in the third report[3], the signal processor is required to work effectively even though the returning acoustic signals may suffer from high levels of clutter (*i.e.*, sediment surface and volume reverberation) and noise.

In order for a detection system to be effective, it should be sensitive to the scattering characteristics of the targets. One way of achieving this is to ensure that the operational bandwidth of the detection system encompasses any maxima in the scattering spectrum of the targets in the burial medium. Hence, the classical scattering theory for plane waves incident on cylinders and spheres (the target types considered in this investigation) is presented in section 3.

Section 4 describes a series of measurements with real objects buried in the laboratory tank. A range of signal processing operations are performed on each set of acquired

---

[1] T G Leighton and R C P Evans, Studies into the detection of buried objects (particularly optical fibres) in saturated sediment. Part 1: Introduction. *ISVR Technical Report No.* 309 (2007).

[2] T G Leighton and R C P Evans, Studies into the detection of buried objects (particularly optical fibres) in saturated sediment. Part 2: Design and commissioning of test tank. *ISVR Technical Report No.* 310 (2007).

[3] R C P Evans and T G Leighton, Studies into the detection of buried objects (particularly optical fibres) in saturated sediment. Part 3: Experimental investigation of acoustic penetration of saturated sediment. *ISVR Technical Report No.* 311 (2007).

data. These encompass, specifically, optimal filtering, and synthetic aperture techniques. A comparison of these different approaches is made in section 4.5.

(There is a preliminary study which examines a simple scattered power measurement, using pulsed AM waveforms, but this can only be seen as rudimentary preparatory work because: (i) it cannot be compared with the waveform dependent filtering methods because it uses a different incident waveform; and (ii) the designers of a realistic system would almost certainly consider some form of matched filter, at the very least an attempt would be made to match the filter input bandwidth to that of the signal).

2 Optimum Detection

For a remote imaging system to be most effective, particularly in a noisy or cluttered environment, its design must be centred around the target being sought and the transmission medium. Careful design of the transducers and the output waveform are important with regard to maximising the interaction between the detection system and the target. These issues have been addressed by Daniels in the field of sub-surface radar, although many of the signal / system design and signal processing topics he discusses apply equally well to sonar [1, 2].

Some waveform design issues are addressed below. These involve the choice of a type of modulation that will maximise the likelihood of detecting a target in the insonified volume. In addition, a number of signal processing techniques are presented that can improve the signal-to-noise ratio of received signals (defined as the ratio of the amplitude of the signal to the mean amplitude of the noise [3]).

2.1 Modulation Methods

The choice of modulation type depends on the particular requirements of penetration depth, resolution, known target characteristics, data processing, system size and cost. Most techniques can be classified in four broad categories [1]: amplitude modulation (AM); frequency modulated continuous wave (FMCW); continuous wave (CW); and pulse expansion / compression methods.

- **Amplitude Modulation.** Two types of AM transmissions may be utilised: a pulse modulated carrier that has a relatively narrow transmission bandwidth; and 'baseband' (defined as the frequency band occupied by all the transmitted modulating signals) pulses that can have a much larger bandwidth and are suited to shallow, high resolution probing.

  AM can provide real time output, without the need for signal processing to derive basic information. However, performance can be limited by time jitter between the transmitter and the receiver unless the time stability of the sampling system is very good [1]. The linearity of the timebase is important in reducing ranging errors and to allow any subsequent pulse-shape-dependent filtering to be performed.

  One of the advantages of AM equipment is that it can be made to be small, and it is less expensive than equipment that involves synthesised sources. However, difficulties arise in matching the transmitted spectrum to the characteristics of the target and the attenuation of the medium.

- **Frequency Modulated Continuous Wave.** For shallow targets requiring a large bandwidth, FMCW methods are an alternative to the use of baseband pulses. The transmitted signal is continuously swept in frequency and the received signal is mixed with a sample of the transmitted one to give a difference frequency. This frequency depends on the time delay, and hence range, of the buried target [1].

  The implementation of FMCW systems requires careful control of the frequency sweep and of the mixing process. In particular, it is necessary for the sweep to be linear in time to minimise degradation due to spectral broadening, and pure and stable in frequency output to avoid the generation of modulation products in the mixer. For effective signal processing, the stability required can only be obtained from synthesised frequency sources. If this is the case then the transmitted spectral shape is easier to control and a wide dynamic range is available. There is a drawback, however, in that these systems can be large and expensive, especially when synthesised sources are used. There is also an inherent need for signal processing to recover the time waveform for interpretation.

- **Continuous Wave.** Continuous, single-frequency transmission can provide a simple approach to the detection of buried objects, requiring only a basic signal

generation system and very little in the way of post-processing. In more advanced systems, transmitting either a single frequency or a few well spaced frequencies accompanied by amplitude and phase measurements over the ground surface, subsurface holographic imaging techniques can be used [4].

- **Pulse Expansion / Compression Techniques.** The total power that can be transmitted in a single pulse is restricted by the peak power output limitations of the source. Greater total power may be transmitted without losing range resolution by using a waveform in which the frequency varies rapidly in a much shorter time than the total transit time to and from a target. For example, the linear-swept FM waveform can have a similar magnitude spectrum to a very short pulse, but can be time-expanded to any duration by modification of its phase spectrum [5].

  Compression of an extended chirp back to a short pulse can be performed by the use of a matched filter after reception. Such filters are often implemented using lumped electrical elements, or using signal processing electronics. There are some novel alternatives such as 'surface acoustic wave' devices, which are in common use for pulse compression applications, *e.g.*, as filters in television sets [6, 7].

Continuous wave systems are capable of accurate velocity measurement. Conversely, pulsed systems are capable of accurate range measurement and resolution. Velocity measurement is not of primary concern in this investigation. Continuous wave systems also have a drawback in that they cannot be used in reverberant environments, such as in the laboratory tank or in real seabeds at high signal levels, since back-reflected energy will dominate at the receiver.

Pulsed AM waveforms have some advantages both the laboratory environment and in the field. They are particularly suited to high-resolution probing, but may lack the power necessary to resolve a target buried at any significant depth. They are used in this investigation (section 4.2) purely for illustrative purposes. The main investigation of this report concerns the use of pulse compression techniques to improve the resolution of the system at greater depths (section 4.3).

2.2 Signal Processing

The aim of signal processing in this investigation is to produce a three-dimensional representation of the subsurface volume. When assessing a particular signal processing technique it is important to consider the effect that noise and clutter will have on the data. The following time-domain techniques may be applied to acquired waveforms, as a first step in reducing noise and clutter, before proceeding with more advanced signal processing operations [1]:

- **Noise Reduction by Averaging (Stacking).** The noise-power-bandwidth of a received waveform may be reduced by $(n_m t)^{-1}$ by taking the unweighted mean of n_m measurements spaced in time, t. If a sufficient number of records are stored then weighted averaging may be performed to equalise the noise and signal bandwidths. This technique reduces random noise but has no effect on clutter.

- **Clutter Reduction by Subtracting the Mean.** It is often reasonable to assume that material properties vary randomly about a location-independent mean. Therefore, the mean of a large number of measurements of a similar medium made at different locations is a measure of system clutter, *i.e.*, reverberation, scatter, *etc*. The subtraction of clutter from individual measurements may then give a set of waveforms in which a reflective target is more visible.

  What cannot be known in any practical situation is the variation in the properties of the ground material. Some statistical estimates can be made, but this clutter reduction method is only applicable when the statistics of the ground are position-independent. The problem could be overcome if the ground were homogeneous, as the detection system could be moved to a location where no target was present and a calibration obtained. It is because this operation is not usually possible that other methods must be found.

- **Time-Varying Gain.** A weighting function may be applied to a received waveform to compensate for attenuation, which is a function of path length in the medium. The disadvantage of this technique is that system noise can also be exaggerated, increasing the difficulty of interpreting the results. A realistic approach is to apply a gain reduction at short time values to suppress surface

reflection signals, followed by a gain increase up to some maximum value. This makes most effective use of the data presentation medium.

- **Frequency Filtering.** It is common to employ low-pass, high-pass and band-pass filters to remove signals outside the system bandwidth, so improving the overall signal-to-noise ratio.

2.3 Advanced Techniques

None of the processes described above require prior knowledge of the transmitted waveform, the target or the noise and clutter in the medium. When such information is available, much more effective target detection techniques can be used.

2.3.1 Waveform Dependent Methods

If it is assumed that an estimate of the incident waveform is available through a calibration experiment or modelling, a filter can be designed to pick out the signal in the received waveform. Such a filter can modify the shape of the received signal, usually into a single peak, to increase the detection probability. An obvious method of doing this is by Wiener filtering [8], where the desired output shape is used as an input to the filter design process. The use of the Wiener filter as an optimal estimator is considered in greater detail in section 4.3.

2.3.2 Target Dependent Methods

The distinctive scattering properties of some targets can be used as a detection aid. In particular, regularly shaped objects (such as spheres and cylinders) have a set of resonances which impose a characteristic spectrum on the scattered signal when illuminated with broadband radiation. For example, the echoes generated from a smooth, solid, elastic cylinder insonified by a source of plane acoustic waves comprise diffracted waves, surface flexural waves and back-reflected compressional waves from within the target [9]. The scattered signal is dependent on the physical dimensions of the target and the mechanical properties of the material from which it is made.

3 Scattering from Cylinders and Spheres

The repeated reflections of propagating acoustic waves from the boundaries of objects of limited size cause constructive interference at certain discrete frequencies. Constructive interference allows the formation of self-sustaining standing waves, known as the 'eigenvibrations' of the object. The infinite set of frequencies that excite these eigenvibrations are called the 'eigenfrequencies' of the object.

If the frequency of an incident acoustic wave coincides with one of the eigenfrequencies of a buried object, the corresponding eigenvibration will be excited. This will affect the scattering process of the incident wave, not least by the fact that energy will be removed from the wave to set up the vibration [9, 10, 11].

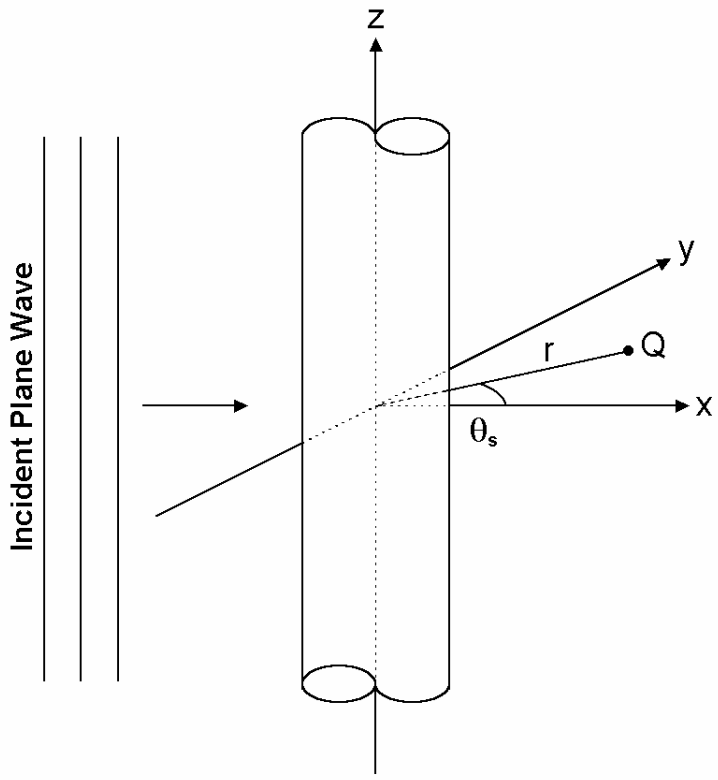

Figure 1 *The geometry used for formulating the problem of sound scattering from an infinite circular cylinder.*

It is common to use a quantity called the form function to describe the steady-state pressure amplitude of a scattered wave [12]. (This parameter is introduced in section 2.2.3 of the second report in this series[2], in the context of scattering from suspended

particles.) It is defined as being the ratio of the angle-dependent amplitude of a scattered wave to the amplitude of an incident wave in the limit as the distance from the scatterer approaches infinity. It is derived by means of a partial wave expansion which contains all the physical features of the solution (reflected waves, circumferential waves and transmitted waves) [13]. It is customary to normalise the form function to unity in the high-frequency limit. Other researchers have reported good agreement between the theoretical form function, obtained using partial wave theory, and experiment both under laboratory conditions and in the field [14, 15].

To determine the set of characteristic resonances of a cylindrical target, consider the scattering geometry depicted in figure 1. An infinite plane acoustic wave, $p_0 \exp\left[j(kx - \omega t)\right]$, with wave number, k, is incident on a solid elastic cylinder of radius, a_c, and density, ρ_c. At a point, Q, located in the fluid of density, ρ_f, surrounding the cylinder it produces the scattered field, p_{sc}.

It should be noted that figure 1 represents an idealised scenario for the detection of buried telecommunication cables, where the vertically-aligned plane of the acoustic transducers is perpendicular to the long-axis of the cable.

If the time dependence, $\exp(-j\omega t)$, is suppressed, the scattered field is given by

$$p_{sc}(r,\theta_s) = p_0 \sum_{n=0}^{\infty} \varepsilon_n j^n R_n(ka_c) H_n^{(1)}(kr) \cos(n\theta_s) \tag{1}$$

where

$$R_n(ka_c) = -\frac{J_n(ka_c)F_n - xJ_n'(ka_c)}{H_n^{(1)}(ka_c)F_n - xH_n^{(1)\prime}(ka_c)}$$

In equation (1), n is the order of the eigenvibration, p_0 is the incident pressure, ε_n is the Neumann factor ($\varepsilon_n = 1$ for $n = 0$, $\varepsilon_n = 2$ for $n > 0$), J_n and $H_n^{(1)}$ are, respectively, Bessel functions and Hankel functions of the first kind and the quantities F_n are related to the modal mechanical impedance of the cylinder:

$$F_n = \frac{\rho_f}{\rho_c}(k_T a_c)^2 \frac{D_n^{(1)}(ka_c)}{D_n^{(2)}(ka_c)} \tag{2}$$

$$D_n^{(1)} = \begin{vmatrix} A_{22} & A_{23} \\ A_{32} & A_{33} \end{vmatrix} \quad \text{and} \quad D_n^{(2)} = \begin{vmatrix} A_{12} & A_{13} \\ A_{32} & A_{33} \end{vmatrix}$$

with elements

$$\begin{aligned}
A_{12} &= \left[(k_T a_c)^2 - 2n^2\right] J_n(k_L a_c) + 2k_L a_c J_n'(k_L a_c) \\
A_{22} &= k_L a_c J_n'(k_L a_c) \\
A_{32} &= 2n\left[J_n(k_L a_c) - k_L a_c J_n'(k_L a_c)\right] \\
A_{13} &= 2n\left[J_n(k_T a_c) - k_T a_c J_n'(k_T a_c)\right] \\
A_{23} &= n J_n(k_T a_c) \\
A_{33} &= \left[(k_T a_c)^2 - 2n^2\right] J_n(k_T a_c) + 2k_T a_c J_n'(k_T a_c)
\end{aligned}$$

The elements of the two 2×2 determinants contain functions with arguments $k_L a_c = \omega a_c / c_L$ and $k_T a_c = \omega a_c / c_T$ where c_L and c_T are, respectively, the speeds of longitudinal and transverse waves in the cylinder material.

In the far-field, where $r >> a_c$, $H_n^{(1)}(kr)$ may be written in asymptotic form:

$$H_n^{(1)}(kr) \approx \sqrt{\frac{2}{\pi kr}} \exp\left(jkr - \frac{jn\pi}{2} - \frac{j\pi}{4}\right) \tag{3}$$

Therefore, the far-field scattered pressure is

$$p_{sc}(\theta_s) = p_0 \exp(jkr) \sqrt{\frac{2}{j\pi kr}} \sum_{n=0}^{\infty} \varepsilon_n R_n(ka_c) \cos(n\theta_s) \tag{4}$$

For monostatic reflection, $\theta_s = \pi$, this becomes

$$p_{sc}(\pi) = p_0 \exp(jkr) \sqrt{\frac{2}{j\pi kr}} \sum_{n=0}^{\infty} \varepsilon_n R_n(ka_c) \cos(n\theta_s) \tag{5}$$

This may be expressed in terms of the far-field form function, $f_\infty(\theta_s)$, which gives a non-dimensional representation of the scattered pressure:

$$f_\infty(\theta_s) = \sqrt{\frac{2r}{a_c}}\frac{p_{sc}}{p_0}\exp(-jkr) \tag{6}$$

Therefore, from equation (5),

$$f_\infty(\theta_s) = 2\sqrt{\frac{1}{j\pi ka_c}}\sum_{n=0}^{\infty}\varepsilon_n R_n(ka_c)\cos(n\theta_s) \tag{7}$$

$$\text{and} \quad f_\infty(\pi) = 2\sqrt{\frac{1}{j\pi ka_c}}\sum_{n=0}^{\infty}\varepsilon_n R_n(ka_c)(-1)^n$$

with the individual normal modes that make up the form function defined as

$$f_n(\theta_s) = 2\sqrt{\frac{1}{j\pi ka_c}}\varepsilon_n R_n(ka_c)\cos(n\theta_s) \tag{8}$$

$$f_\infty(\theta_s) = \sum_{n=0}^{\infty} f_n(\theta_s)$$

There are two limiting cases of this result. If $\rho_c \to \infty$, the solution applies to scattering by a rigid cylinder:

$$R_n(ka_c)_{rigid} = -\frac{J_n'(ka_c)}{H_n^{(1)\prime}(ka_c)} \tag{9}$$

If $\rho_c \to 0$, the solution for a soft cylinder is obtained:

$$R_n(ka_c)_{soft} = -\frac{J_n(ka_c)}{H_n^{(1)}(ka_c)} \tag{10}$$

The resonances associated with the cylinder can be found with the aid of equation (9), referred to as the 'rigid background' case. This describes the Rayleigh scattered field[4] that results from the reflection and diffraction of the incident acoustic waves. Subtracting it from the elastic response leaves the resonance spectrum.

The case of plane-wave acoustic scattering from an elastic sphere of radius, a_s, can be treated as being analogous to that from a cylinder [9]. The scattered amplitude for an incident wave of amplitude, p_0, is

[4] Rayleigh scattering is first introduced in the context of electromagnetic wave scattering in section 3.1.1 of the first report in this series.

$$p_{sc}(r,\theta_s)=p_0\sum_{n=0}^{\infty}(2n+1)j_n r_n h_n^{(1)}(kr)P_n\cos(n\theta_s) \tag{11}$$

where

$$r_n(ka_s)=-\frac{j_n(ka_s)F_n-ka_s j_n'(ka_s)}{h_n^{(1)}(ka_s)F_n-ka_s h_n^{(1)\prime}(ka_s)}$$

In equation (11), j_n and $h_n^{(1)}$ are, respectively, spherical Bessel functions and spherical Hankel functions of the first kind and P_n are the Legendre polynomials [16]. In this case, the real quantity, F_n, as given by Hickling [17], contains spherical cylinder functions with arguments $k_L a_s$ and $k_T a_s$. It is proportional to ρ_f/ρ_s where ρ_s is the density of the sphere:

$$F_n=\frac{\rho_f}{\rho_s}\frac{(k_T a_s)^2}{2}\frac{D_n^{(1)}(ka_s)}{D_n^{(2)}(ka_s)} \tag{12}$$

$$D_n^{(1)}=\begin{vmatrix}A_{22} & A_{23}\\ A_{32} & A_{33}\end{vmatrix} \quad \text{and} \quad D_n^{(2)}=\begin{vmatrix}A_{12} & A_{13}\\ A_{32} & A_{33}\end{vmatrix}$$

with elements

$$A_{12}=(k_L a_s)^2\left[(\upsilon/1-2\upsilon)j_n(k_L a_s)-j_n''(k_L a_s)\right]$$
$$A_{22}=k_L a_s j_n'(k_L a_s)$$
$$A_{32}=\left[(n^2+n-2)j_n(k_T a_s)+(k_T a_s)^2 j_n''(k_T a_s)\right]^{-1}$$
$$A_{13}=2(n^2+n)\left[j_n(k_T a_s)-(k_T a_s)^2 j_n'(k_T a_s)\right]$$
$$A_{23}=2(n^2+n)j_n(k_T a_s)$$
$$A_{33}=\left[k_L a_s j_n'(k_L a_s)-j_n(k_L a_s)\right]^{-1}$$

where υ in the above description of A_{12} is Poisson's ratio.

The remaining analysis is similar to that for the cylinder, but with slightly different resonance parameters. The individual modes that make up the form function for the sphere are defined as

$$f_n(\theta_s) = \frac{2}{ka_s}(2n+1)e^{j\delta_n}\sin(\delta_n)P_n\cos(n\theta_s) \tag{13}$$

where

$$\tan(\delta_n) = -\frac{j_n(ka_s)f_n - ka_s j_n'(ka_s)}{n_n(ka_s)f_n - ka_s n_n'(ka_s)}$$

wher n_n are spherical Neumann functions [16].

The scattered pressure is calculated from the superposition of the normal modes that make up the form function on a rigid background. The rigid background is equivalent to the Rayleigh scattering case with none of the elastic modes that penetrate the sphere. Therefore, as in the previous case for a cylinder, this expression can be thought of as consisting of resonances superimposed on an 'impenetrable background'.

3.1 Form Function Calculation

The form function has been calculated for three different kinds of buried target: a steel cylinder; a polyethylene cylinder; and a steel sphere. The material bulk properties required for the form function calculations are listed in table 1. These target types were of particular interest in this investigation for a number of reasons:

- Steel has a large acoustic impedance mismatch with the host sediment (pressure amplitude reflection coefficient, $R_{Pa} = 0.86$, from equation (12) of the second report in this series[2], with $\theta_i = \theta_t = 0$), so making it a useful baseline material for a test target.

- Conversely, polyethylene in principle makes a more 'difficult' target, because it has a small acoustic impedance mismatch compared with the sediment (pressure amplitude reflection coefficient, $R_{Pa} = -0.34$, from equation (12) of the second report in this series[2], with $\theta_i = \theta_t = 0$).

- A spherical target is also useful because burial and retrieval is easier to perform and causes less disturbance to the sediment than is the case for a cylindrical target.

It is important to note that the sediment was assumed to behave like a fluid medium. (In section 2.2.5 of the second report in this series[2], it is noted that this assumption is usually valid for most sediment types. The sediment as a poro-elastic medium is

considered in more detail in the third report in this series[3], where the nature of the rough water-sediment interface is examined). The validity of using classical scattering theory when the surrounding medium is not a true fluid has not been addressed in detail in this investigation.

However, it is likely that the scattering function associated with targets buried in the laboratory tank (described in the second report in this series[2]) will be somewhat different in practice to that predicted by the theory presented earlier in this section. This is partly because radiation loading from the surrounding medium results in a high damping constant for resonant vibratory modes, which would otherwise be good radiators of sound. As a consequence, these modes do not necessarily give rise to an increase in target strength. In fact, it is possible that resonant modes may be accompanied by a lower target strength if high internal losses cause significant absorption of the incident energy [18].

In this study, an exact scattering model may not be necessary to fulfil the objective of detecting buried objects. It has been assumed that the form function approximations, derived above, should be close enough to reality to allow the unambiguous detection of buried spheres and cylinders. This is tested in the section 4 of this report, an experimental investigation into the detection of buried objects.

Parameter	Sediment	Steel (1 % C)	Polyethylene
Longitudinal wave speed (m s^{-1})	1 692	5 940	1 950
Transverse wave speed (m s^{-1})	-	3 220	540
Density (kg m^{-3})	2 107	7 840	900
Poisson's ratio	-	~ 0.30	-

Table 1 *The bulk parameters used in the calculation of the form functions for spherical and cylindrical scatterers immersed in a sediment medium.*

For a target of characteristic radius a_t, the results from the form function calculations as a function of the non-dimensional acoustic frequency, ka_t, are shown in figure 2.

The scattering angle, $\theta_s = 104°$, corresponds to the angle of scattering in the laboratory test facility, according to the arrangement of the apparatus detailed in the second report in this series[2]. It should be noted that additional mechanical damping has not been included in the form function calculation.

For the steel cylinder (case a) and the polyethylene cylinder (case b), the form function is plotted up to $ka_t = 6$. For the steel sphere (case c), the form function is plotted up to $ka_t = 12$. These frequency ranges correspond to the frequency band from DC to approximately 150 kHz for a set of real targets having radii of 1.25 cm in case a, 1 cm in case b, and 2.5 cm in case c. This frequency band covers the maximum operational bandwidth of the transducers used in the test facility.

The resonances associated with each target cause the differences between the elastic and rigid background cases. The steel targets do not exhibit any really distinct resonances. Conversely, resonances are particularly distinct for the polyethylene target, which is a more compressible material than steel. This suggests that a resonance-based detection system may have a good chance of finding high compressibility materials, whereas a detection system that is only capable of detecting changes in the scattering level may be better suited to finding low compressibility materials. (The compressibility of the target material is also of interest with regard to telecommunication cables and the acousto-optic effect, as detailed in section 5 of the fifth report in this series[5].)

[5] R C P Evans and T G Leighton, Studies into the detection of buried objects (particularly optical fibres) in saturated sediment. Part 5: An acousto-optic detection system. *ISVR Technical Report No.* 313 (2007).

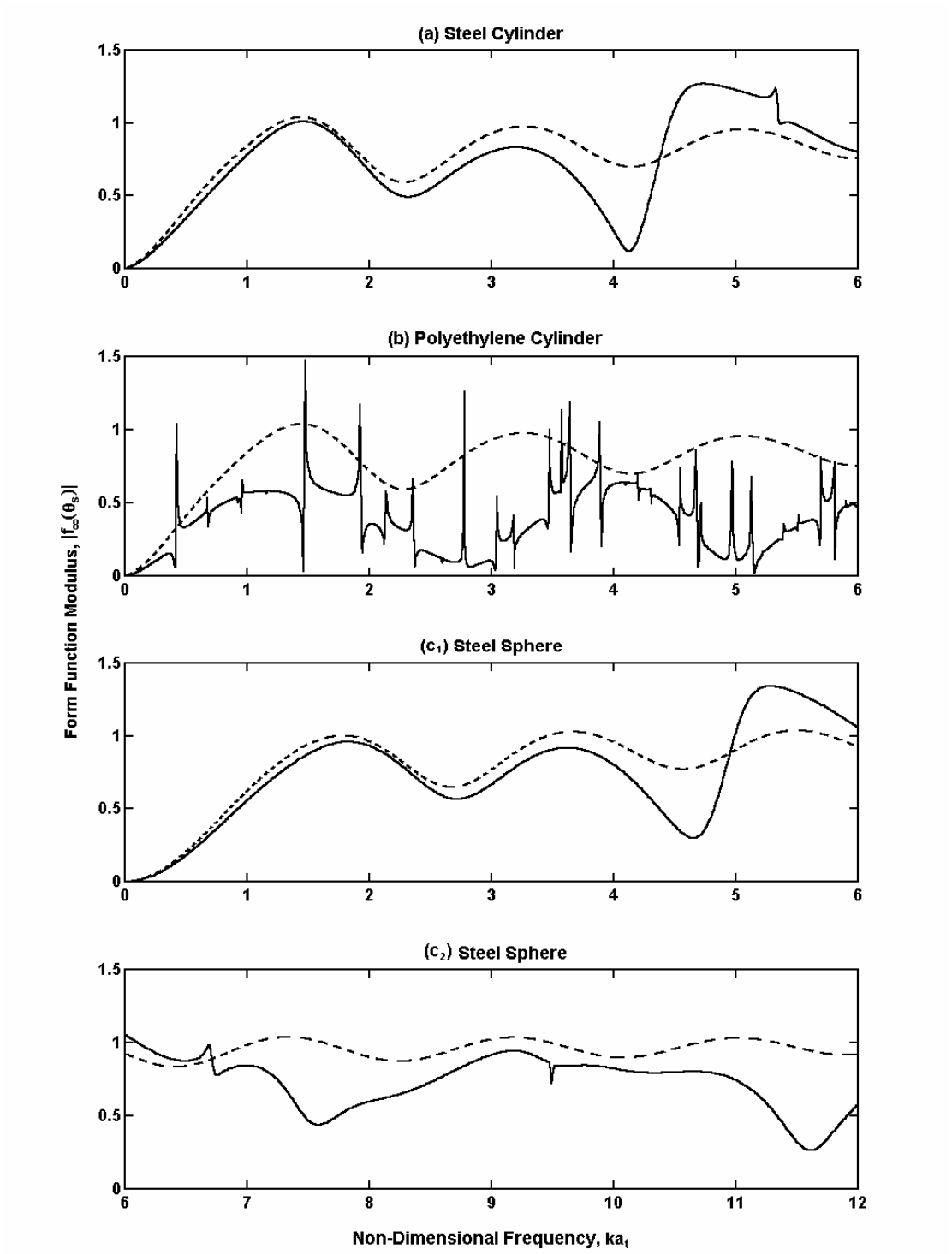

Figure 2 *The solid curves are the form function moduli at scattering angles,* $\theta_s = 104°$*, for (a) a steel cylinder, (b) a polyethylene cylinder, and (c) a steel sphere as functions of non-dimensional frequency. The dashed curves are the corresponding form function moduli for the rigid background cases. (For clarity, (c) is plotted over two graphs since the frequency range is twice that used for (a) and (b)).*

3.2 Combined System Response

Ordinarily a minimum resolution requirement for a detection system would be that $ka_t > 1$ since frequencies below this limit result in significantly less scattering. This assumes that the effect of the attenuation associated with the burial medium is insignificant. In the second report in this series[2], it was noted that the attenuating effects of seawater, and of clouds of suspended material are small compared to the attenuating effect of the sediment and may be regarded as being insignificant. However, the attenuation coefficient of the sediment in the laboratory tank is significant, scaling almost linearly as the first power of frequency and being in excess of 10 dB m^{-1} over the range of frequencies of interest in this investigation (see section 2.2.4 of the second report in this series[2]).

The normalised back-scatter cross-sections [9, 19] for two rigid targets, a sphere and a cylinder, were calculated[6]. These results are plotted as a function of acoustic frequency in figure 3 (red curves). The slopes of the curves in the Rayleigh scattering regime ($ka_t << 1$) correspond to the scattering geometry of the targets: the spherical scatterer has a slope of 40 dB per decade; and the cylindrical scatterer has a slope of 30 dB per decade (12 dB per octave and 9 dB per octave, respectively).

The effect of the attenuation of sound in the medium (by absorption, scattering, *etc*.) may be combined with the back-scatter cross-section to give the effective normalised back-scatter. This is a normalised measure of the fraction of the transmitted signal returned to the receiver after it has been attenuated within the medium and scattered by the target. The calculation is performed by subtracting the value of attenuation in decibels from the back-scatter cross-section of the target. Unfortunately, it is not possible to generalise the result to obtain an effective back-scatter function that scales with the non-dimensional frequency, as is the case for the back-scatter cross-section. This is because attenuation is not only dependent on frequency, but on the acoustic path length in the medium.

---

[6] The back-scatter cross-section is related to the form function, being the ratio of re-radiated to incident acoustic intensity at a distance of 1 m from the scattering centre of the target. If it is normalised to remove its geometrical dependence, it becomes $|f_\infty(\pi)^2|$. For a sphere, the normalisation factor is πa_t^2, and for a cylinder it is $2\pi a_t$.

Original in colour

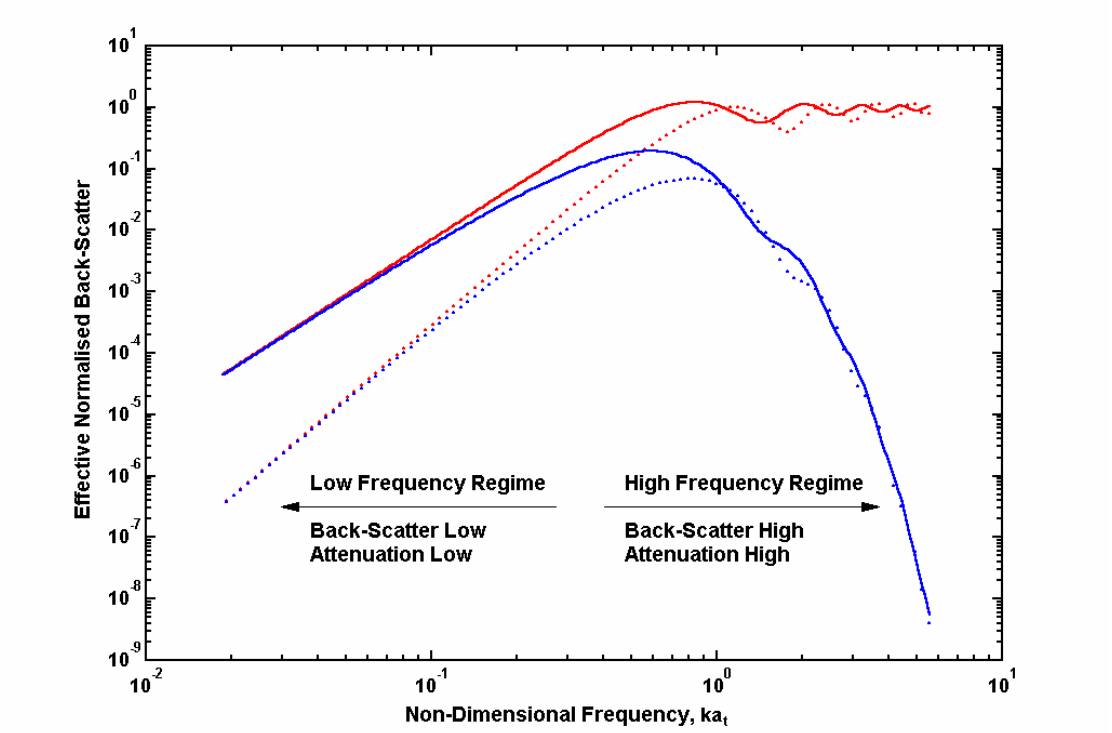

Figure 3 *The red curves are the normalised back-scatter cross-sections for a rigid sphere (dotted curve) and a rigid cylinder (solid curve), calculated for a medium that does not absorb sound. The blue curves show the effective normalised back-scatter, where the effect of attenuation in the surrounding medium is included for the sphere (dotted curve) and the cylinder (solid curve). It is assumed that both targets have radii of 1 cm, the acoustic path length is 1 m, and the speed of sound is 1 692 m* s^{-1}.

An example, illustrating the effect of including attenuation in the calculation has been produced. A scatterer radius of 1 cm was chosen as being typical of the dimensions of the targets that are of interest in this investigation (and similar to the dimensions of the real targets that were used in the experiments detailed in the following sections). The speed of sound in the sediment was known to be 1 692 m s^{-1} ± 2 % (see section 2.2.1 of the second report in this series[2]). For a burial depth of between 25 cm and 30 cm, the path length in the sediment was known to be around 1 m. (For the purpose of this example, it was assumed to be exactly 1 m.) Thus, for the given radius, sound speed and path length, the responses for a rigid sphere and cylinder were calculated.

The results of these calculations are plotted as functions of acoustic frequency in figure 3 (blue curves). Frequency has been converted into a non-dimensional form for the purpose of allowing a direct comparison with the previous result. The curves shown in the figure span the frequency range from 500 Hz to 150 kHz, with $ka_t = 1$ corresponding to a frequency of around 27 kHz (in fact $26\,929 \pm 2$ %, with the associated error corresponding to the uncertainty in the sound speed measurement).

It is clear that when attenuation is included, the resolution requirement is no longer as simple as $ka_t > 1$. In fact, at higher frequencies the back-scattered signal is considerably less than for frequencies corresponding to $ka_t << 1$. In terms of maximising the back-scattered signal at the receiver, an optimal frequency band can be selected given the target size, range, and the attenuation of the medium. For the simple case presented above, a detection system operating at a centre frequency of around 27 kHz would seem to be a good choice.

An important aspect of a practical detection system that has not yet been considered is the response of the detection system hardware. The laboratory system, detailed in the second report in this series[2], included signal generation / data acquisition electronics, a power amplifier, a charge amplifier, *etc.*, all of which displayed a reasonably flat response over the DC to 150 kHz frequency range. The acoustic transducer elements also displayed a reasonably flat response when acting as receivers. However, when used as transmitters they exhibited a steep, 40 dB per decade increase in sound pressure level in response to driving voltage, and a distinct resonance at around 120 kHz. When this response is taken into consideration, the importance of higher frequencies (*i.e.*, frequencies corresponding to $ka_t > 1$) is re-established.

Thus far, this discussion has dealt with achieving the maximum scattered signal at the receiver. It is important to remember that, in a real system, it is the signal-to-noise ratio that must be maximised. In the laboratory environment there is considerable scope to ensure low-noise conditions, by repeated averaging of data and isolation of background sources. In the field, however, noise contamination at the receiver is unavoidable and demands further attention.

There are three basic classes of noise [20]: electrical noise, which should be negligible in a well designed system; self-noise from the ROV, *etc.*, which can be

troublesome (although it can be reduced with careful transducer design); and ambient noise. The sources of ambient noise are both natural and human-made, with different sources exhibiting different spectral characteristics [21]. Natural sources of noise include seismic disturbances, wind-wave interaction, thermal activity of the water molecules, as well as biological sources such as snapping shrimp, dolphins, and various other fishes and ocean mammals. The principal human-made component of ambient noise is often the sound generated by shipping.

Ambient noise in the deep ocean can be divided into three spectral bands [21, 22]. The low-frequency band covers the range from less than 1 Hz to about 500 Hz. Ambient noise in this band is dominated by the sounds of distant shipping. The mid-frequency band extends to about 50 kHz and is dominated by the effects of wind acting on the sea surface. Knudsen demonstrated a correlation between ambient noise and wind force [23]. Wind related noise has a broad spectral peak and decreases at a rate of 5 - 6 dB per octave at higher frequencies. In the frequency band above 50 kHz, ambient noise is dominated by the thermal agitation of the water molecules. This component of noise increases at 6 dB per octave.

The minimum noise level in the ocean occurs at a frequency of around 100 kHz. If this is taken into consideration, the importance of the higher frequencies in the optimal frequency band is further emphasised [24]. Therefore, for the experiments in the following sections, it was thought sensible to use frequencies covering the whole operational range of the transducers (*i.e.*, from around 20 kHz to 120 kHz). This range extends down to the frequencies at which scattering is a maximum for the targets considered, without excluding the higher frequencies which are important when the system response and the ocean ambient noise spectrum are taken into account.

4 The Detection of Buried Objects

The detection tests will compare the effectiveness of various waveform dependent filtering methods which use FM waveforms suitable for pulse compression. The target and volume scattering information presented in section 3 can be used to implement target dependent processing techniques.

That main study is preceded by a preliminary study which examines a simple scattered power measurement, using pulsed AM waveforms, but this can only be seen as rudimentary preparatory work because: (i) it cannot be compared with the waveform dependent filtering methods because it uses a different incident waveform; and (ii) the designers of a realistic system would almost certainly consider some form of matched filter, at the very least an attempt would be made to match the filter input bandwidth to that of the signal.

4.1 Experimental Arrangement

The experimental apparatus, comprising a water tank part-filled with sediment and a pair of focused acoustic transducers, is described in the second report in this series[2]. The acoustic axes of the transducers were inclined at an angle of incidence of 33° ± 2°, and aligned such that they would intersect at discrete sample points within the sediment. Thus, each set of data comprised a series of pulse-echo measurements from a range of sample points.

At first, it was estimated that a sample spacing of around 5 cm would give adequate coverage of the target volume when searching for cm-scale targets. From the directional characteristic of the transducers in the sediment (measured in section 3 of the second report in this series[2]) it can be seen that the sound power on the acoustic axis is reasonably uniform across this width. Also, this is greater than the ± 1 cm error associated with the position control apparatus, described in section 4 of the second report in this series[2].

Using the scanning pattern for the position control rig (described in section 4 of the second report in this series[2]), a sample spacing of 5 cm resulted in there being 60 points in each sample plane within the sediment. Using a test target, measurements were taken from five planes spaced 5 cm apart, giving a total of 300 sample points. In the course of the experiments detailed in the following sections, it was found that the resolution associated with this sample spacing was not always high enough to provide conclusive detection results. Therefore, many of the experiments were repeated with a reduced sample spacing, such that there were 300 points in each sample plane within the sediment.

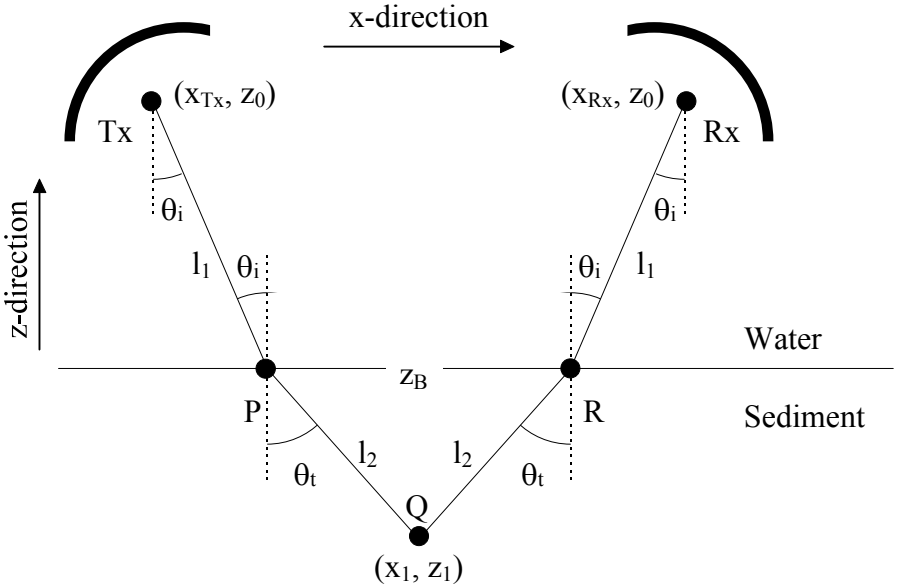

Figure 4 *The acoustic path from the source, Tx, to the intersection point within the sediment, Q, and back to the receiver, Rx.*

Targets were buried at a depth of between 25 cm and 30 cm in the sediment and near to the middle of the tank. This position corresponded, approximately, to the centre of each sample plane. Four different targets were used in the investigation: a steel sphere, 50 mm in diameter; a steel cylinder, 25 mm in diameter; a polyethylene cylinder, 20 mm in diameter; and a section of real, lightweight telecommunication cable, 22 mm in diameter. The reasons for using each of these target types are noted in section 3.1. The cylinders were oriented so that their long-axes were perpendicular to the sample planes, *i.e.*, each plane sliced through a cross-section of a cylinder.

The time-of-flight (TOF) of an output acoustic pulse (travelling from the source element to the sample point and back to the receiver element) was required for the processing operations described in the following sections. This geometry is summarised in figure 4 and allows a reasonable estimate to be made for the time-of-flight of a pseudo-plane-wave pulse travelling parallel to the acoustic axes of the transducers.

The source and receiver transducers are denoted Tx and Rx. Given the positions of the acoustic elements, (x_{Tx}, z_0), (x_{Rx}, z_0), the height of the water-sediment boundary, z_B, the position of the sample point, (x_1, z_1), and the speeds of sound in the water and sediment, c_w and c_s, respectively, the calculation is quite straightforward. It should be noted that the acoustic paths from the acoustic elements to the reflectors have not

been drawn on the diagram for clarity but they are included in the time-of-flight calculation:

$$\mathrm{TOF} = 2\left(\frac{2S_0}{c_w} + \frac{z_0 - z_B}{c_w \cos\theta_i} + \frac{z_B - z_1}{c_s \cos\theta_t} \right) \tag{14}$$

where S_0 is the separation between the acoustic elements and the back of the reflectors.

As discussed in detail in the third report in this series[3], surface roughness can cause significant scattering of acoustic energy at the water-sediment interface. Roughness scattering was expected to cause some error, by way of blurring the volume being focused upon by the transducers, although the extent of this error is difficult to quantify. However, the assumption of a 'smooth' interface[7] in the above calculation was still expected to give a reasonable estimate of the time-of-flight through the centre of the focal volume. The validity of this assumption is tested in subsequent sections.

The principal source of error in the alignment of the time waveforms was expected to be due to positional errors in the apparatus. For targets buried in the centre of the tank, the TOF was calculated to be around 1.1 ms with a maximum temporal error of around ± 10 μs using the parameters established in the second report in this series[2]. Hence, when it was necessary to apply a time window, a window of at least 20 μs and centred around the TOF was applied to the processed time waveforms.

For the results presented later in this report, a time window of 50 μs was used. The window size was greater than the 20 μs calculated to be the acceptable threshold, in order to ensure that no useful information was being excluded. It was found that the larger window size made little difference to the results; the measured energy of signals associated with the presence of a target was not found to increase appreciably. Any change that was observed was attributed to an increase in the total noise energy

[7] Note that that the rms height of the sediment in the laboratory tank (< 1 mm) corresponded to a nominally smooth interface for the range of frequencies of interest in this investigation. Also, it was noted that the sediment used in the laboratory was similar to that in which submarine cables are buried in the field.

(*i.e.*, the product of the instantaneous noise power and the duration of the time window).

4.1.1 Pre-Processing

The following pre-processing operations were performed on all the received signals before commencing with any signal processing analysis. Some have been mentioned earlier in this report, but they are summarised here for completeness:

- Every waveform that was obtained using the data acquisition system was the average of 100 output pulses, thus reducing the level of the background noise signal by a factor of 10.
- Band-pass filtering in the 20 - 120 kHz range was performed to limit the system bandwidth to the maximum operational bandwidth of the transducers. Signal energy outside of this frequency range carried no useful information and could only have served to increase the noise level.
- The triggering level and pre-triggering delays of the acquisition system were used to align all the measured data within a common time frame. This was necessary to enable subsequent time windowing operations.

4.2 Scattered Power

Prior to the comparisons between target detection techniques in sections 4.3 and 4.4, some initial measurements were made of the scattered power when the four targets were subjected to AM insonification. This tested the ability of the control and data acquisition systems to measure the power in acoustic signals scattered from each sample point within the sediment. With no target in the field-of-view of the acoustic reflectors it was expected that the received waveforms would only contain noise and clutter from the tank and the sediment. Conversely, if there was a reflective target in the field-of-view it was expected that the total power would increase.

The processing method involved first squaring the band-pass filtered returned signals to obtain a value that was proportional to the instantaneous acoustic energy at the receiver. Time windowing was then applied, according to the method described in section 4.1, and the peak value in the window was recorded as the detection result. It

should be noted that this actually gives the peak energy in the returned signal and not the time-averaged power. A power calculation was performed, initially, by summing over the time window. However, very little difference was observed between the results obtained using the two methods, so the simpler processing option was chosen.

In order for this processing method to be effective, a pulsed waveform of short time duration was required. This implied that the waveform would also have broadband characteristics. However, in order to make most efficient use of the detection system, the output waveform had to be band-limited to exist within the operational bandwidth of the transducers. A suitable waveform is the AM baseband pulse, discussed in section 2.1, which is suited to shallow, high-resolution probing.

The output pulse was designed in the frequency domain by defining the magnitude spectrum to be zero everywhere except for the frequency band of interest where it was assigned a constant value. The inverse Fourier transform of this spectrum has the general form of $\sin(\pi x)/\pi x$ and is symmetrical about time, $t = 0$. To force the signal to be causal it was a simple case of selecting a portion of the signal in a time window from $-T_W$ to T_W, and introducing a delay such that time, $t = -T_W$, became $t = 0$.

The truncation of a signal in the time-domain introduces distortion in the frequency spectrum. If the truncation is abrupt, the frequency-domain distortion will exhibit an oscillatory effect that is analogous to 'ringing' in the time-domain. The effects of signal truncation can be mitigated by the use of an appropriate windowing function. For the output pulse considered in this case, the Bartlett (triangular) window was chosen as being the most appropriate. The resulting waveform is shown in figure 5 and has a duration of 50 μs.

With reference to the experimental arrangement described in section 3.1, a sample spacing of 5 cm was used for measurements involving the steel sphere, and a spacing of approximately 2 cm was used for the cylindrical targets. That is to say, the scanning pattern of 60 sample points was for the sphere, and the pattern of 300 sample points was used for the cylinders. The scattered power was calculated from every sample point for each different object. The results are presented in figures 6 to 9.

In each image, the *z*-direction corresponds to vertical position in the sediment, measured upwards from the bottom of the laboratory tank, and the *x*-direction

corresponds to horizontal position. In the case of the buried cylindrical targets, the *x*-direction is perpendicular to their long-axes.

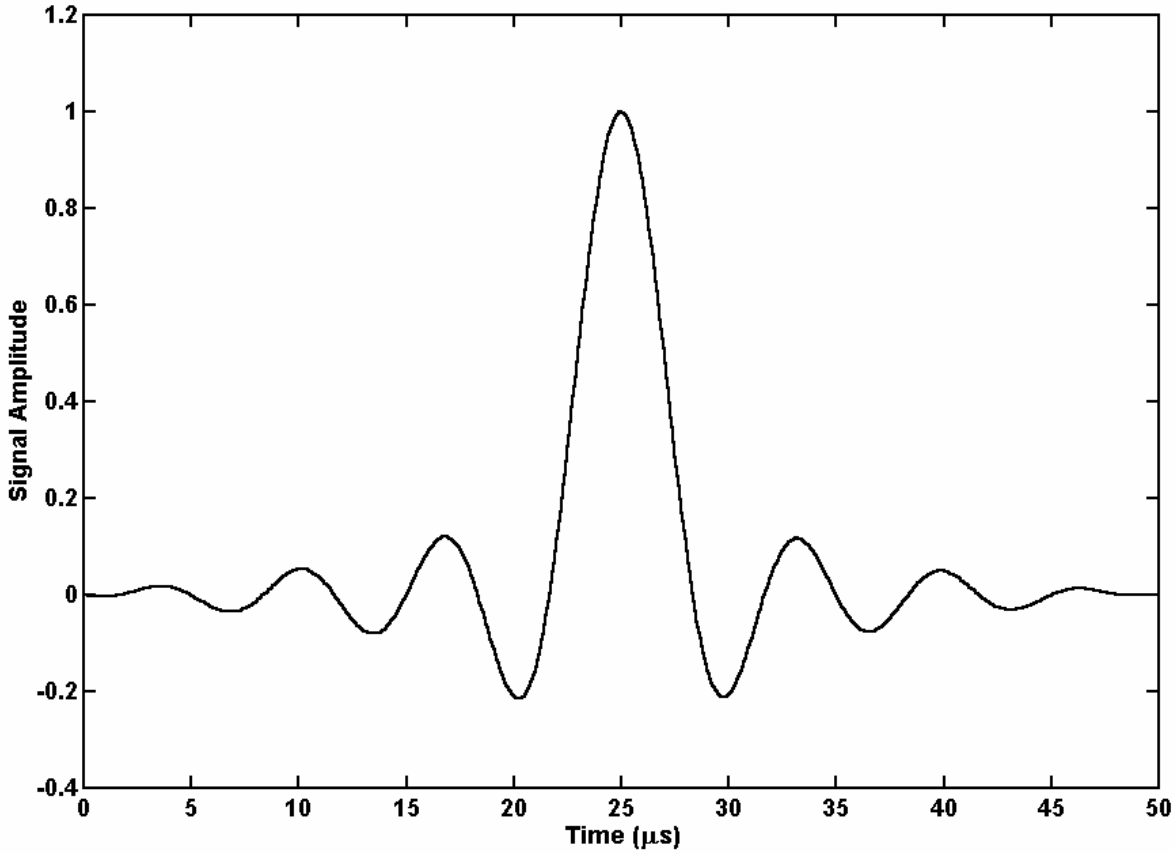

Figure 5 *The time windowed, baseband AM pulse waveform.*

The sample points are marked in each image using the symbol, ×. For the buried sphere, 60 sample points were measured in each of the five vertical planes within the sediment. The processed results were then spatially averaged. For the cylindrical targets, 300 sample points were measured in each of the vertical planes. The processed results are shown without any spatial averaging having been performed. Continuous images were formed by interpolating between each sample point using a piecewise bilinear interpolation algorithm.

The values in each image have been normalised relative to the peak-squared level at the filter output. This level was found to be around 40 kPa^2, with a mean-squared acoustic pressure amplitude of around 1 MPa^2 being generated at each sample point within the sediment.

The signal-to-noise ratio (SNR) was chosen as the figure-of-merit that would allow these results to be compared with alternative processing techniques. It was calculated for each set of measurements by dividing the peak-squared value at the filter output (with no normalisation having been applied) by an estimate of the average noise level. The average noise level was determined by applying similar processing to a set of baseline measurements, which were obtained when the experiment tank contained no buried targets, and calculating the mean-squared value at the filter output. The SNR values that were obtained are noted alongside each of the graphs below.

In each set of data, the scattered power can be seen to increase at a depth corresponding to the target burial region. This could be taken as being indicative of the presence of a buried object. However, the high scattering regions are poorly localised in the horizontal direction. Also, there are a significant number of extraneous points, particularly at shallow depths, that could also be indicative of buried objects. (In the laboratory case, of course, it was known with certainty that there were no targets at these positions. The buried objects were all located centrally in the tank at depths of between 25 cm and 30 cm.) These points arise as a result of volume and reverberant scattering from within the sediment.

Overall, these measurements show a general increase in the scattered acoustic power from the region of each target. However, the presence of a high level of clutter in the filtered output counter-indicates against use of this method, and indeed its use would be naive since designers of a realistic target detection system would almost certainly consider some form of matched filter, at the very least an attempt would be made to match the filter input bandwidth to the bandwidth of the signal.

Having undertaken these preliminary systems tests, sections 4.2 and 4.3 will describe the comparative target detection tests.

Original in colour

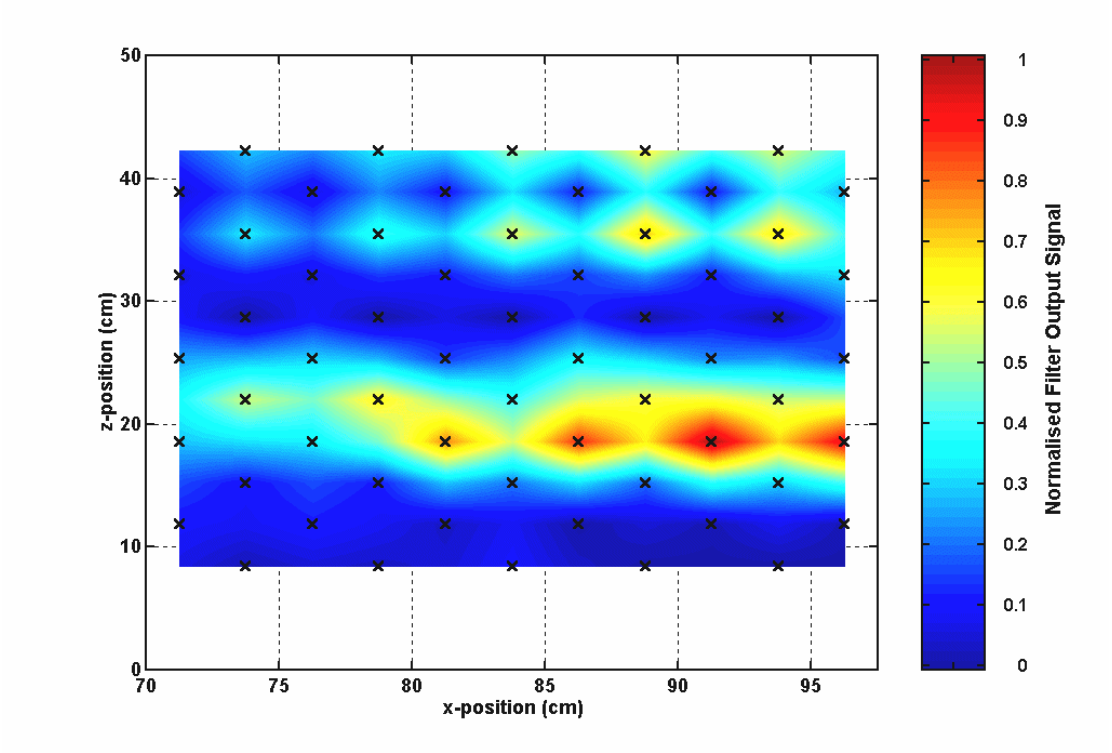

Figure 6 *The normalised, scattered acoustic power from a target region containing a steel sphere (SNR = 18.9 dB).*

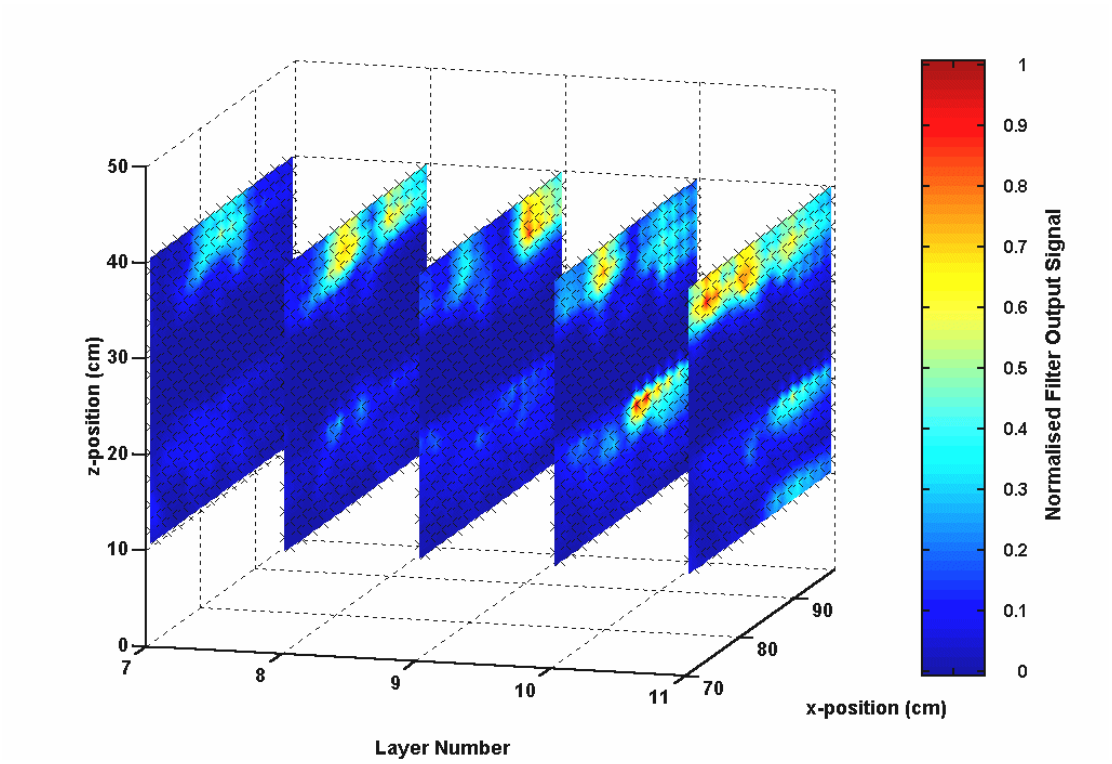

Figure 7 *The normalised, scattered acoustic power from a target region containing a polyethylene cylinder (SNR = 19.1 dB).*

Original in colour

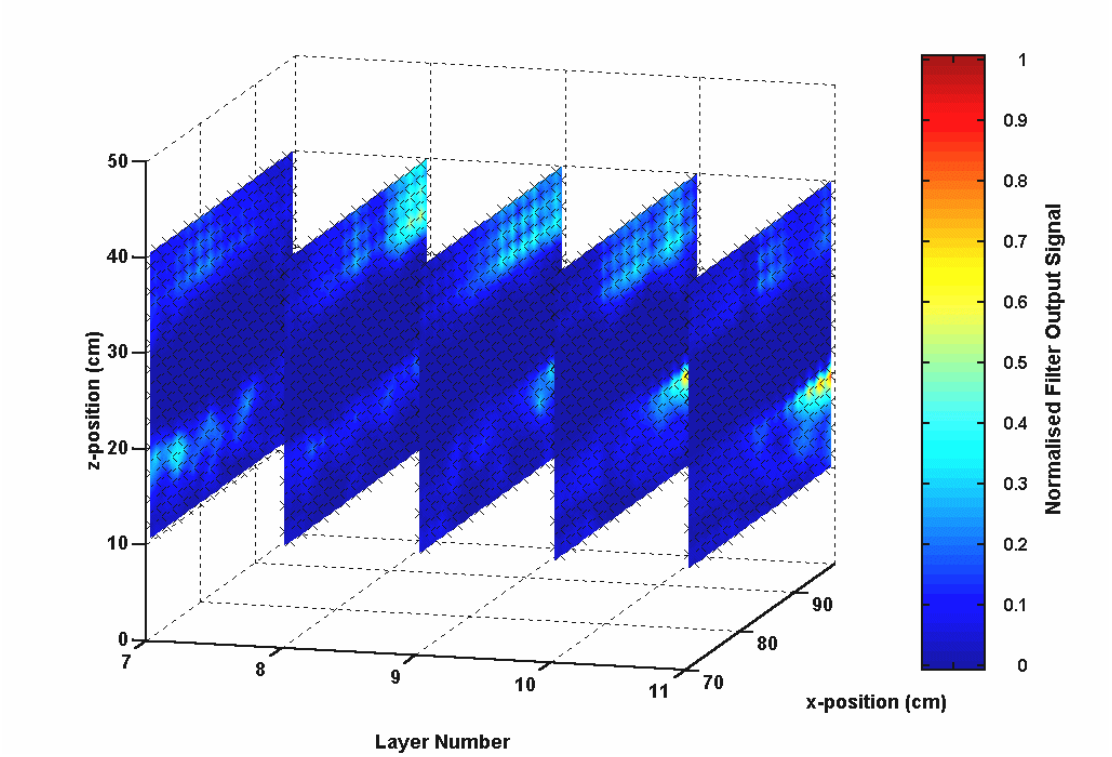

Figure 8 *The normalised, scattered acoustic power from a target region containing a steel cylinder (SNR = 19.5 dB).*

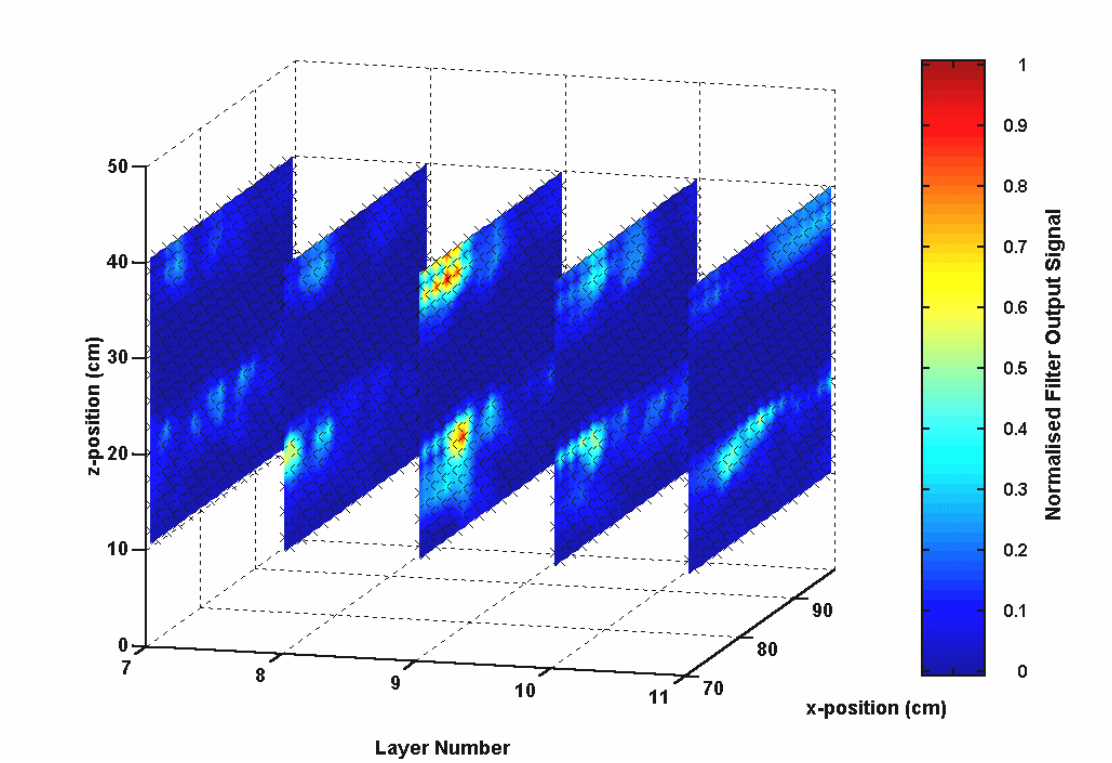

Figure 9 *The normalised, scattered acoustic power from a target region containing a real cable (SNR = 19.9 dB).*

4.3 Optimal Filtering

An optimal filter is one that is designed to select and modify the shape of a signal to maximise the likelihood of detection of any targets that may be present. For measurements containing high levels of noise, such as those obtained in the field, this can be very useful [8]. A sample of the noise spectrum is usually required and can be obtained from calibration measurements.

In general, the frequency response function of a system can be translated into a compact form that involves the measured signal, Q(ω), the noise signal, N(ω), and S(ω) which is the product of the output signal, U(ω), and the response function of the transducers, R(ω) [8]:

$$Q(\omega) = S(\omega) + N(\omega) \quad \text{and} \quad S(\omega) = U(\omega)R(\omega) \tag{15}$$

In the absence of noise, the response function can be deconvolved in the frequency domain by dividing Q(ω) by R(ω). The analogous problem, in the presence of noise, is to find the optimal filter, Φ(ω), which, when applied to the measured signal, Q(ω), and deconvolved by R(ω), will give the signal, $\tilde{U}(\omega)$. This must be as close as possible to the uncorrupted signal, U(ω):

$$\tilde{U}(\omega) = \frac{Q(\omega)\Phi(\omega)}{R(\omega)} \tag{16}$$

Therefore, if U(ω) and $\tilde{U}(\omega)$ are to be as close as possible in the least square sense, it is necessary to minimise the function

$$\begin{aligned} \int_{-\infty}^{\infty} \left|\tilde{U}(\omega) - U(\omega)\right|^2 d\omega &= \int_{-\infty}^{\infty} \left| \frac{\left[S(\omega) + N(\omega)\right]\Phi(\omega)}{R(\omega)} - \frac{S(\omega)}{R(\omega)} \right|^2 d\omega \\ &= \int_{-\infty}^{\infty} \left|R(\omega)\right|^{-2} \left\{ \left|S(\omega)\right|^2 \left|1 - \Phi(\omega)\right|^2 + \left|N(\omega)\right|^2 \left|\Phi(\omega)\right|^2 \right\} d\omega \end{aligned} \tag{17}$$

The components of the signal and the noise are uncorrelated so the integral of their cross-products is zero. Equation (17) is a minimum if the integrand is minimised with respect to Φ(ω). Differentiating with respect to Φ, and setting the result equal to zero, gives the general formula for the optimal filter:

$$\Phi(\omega) = \frac{|S(\omega)|^2}{|S(\omega)|^2 + |N(\omega)|^2} \tag{18}$$

In an advanced system, emphasis must be placed on achieving detection in a near optimum manner. It has been demonstrated that the duration of a transmitted pulse can be as long as necessary to meet any energy requirement, and still meet resolution requirements, if the signal is encoded with wideband modulation information [25]; resolution is a function of the signal bandwidth, and not of the transmitted pulse width. However, to extract information from this type of signal requires a more complex receiving system than that used for a simple pulsed system.

4.3.1 The Matched Filter

A matched filter is a special case of the optimal filter, and constitutes the optimum linear processor for a signal that is corrupted by Gaussian white noise [26]. It transforms the raw data at the receiver into a form that is suitable for performing optimum detection decisions, *i.e.*, target / no target decisions, or the estimation of target parameters with minimum error or maximum resolution.

In the frequency domain, the matched filter transfer function, H(ω), is defined as the complex conjugate of the spectrum of the signal to be processed:

$$H(\omega) = k_n S^*(\omega) \exp(-j\omega T_d) \tag{19}$$

where T_d is a delay constant, required to make the filter physically realisable. As a general simplification, the normalising factor, k_n, and the delay can be ignored to give

$$H(\omega) = S^*(\omega) \tag{20}$$

This can be derived on the basis of the signal-to-noise criterion, which assumes that an optimal system will maximise the signal-to-noise ratio at one instant of time:

$$\begin{aligned} \text{SNR} &= \frac{\text{peak instantaneous signal power}}{\text{rms noise power}} \\ &\equiv \frac{\text{signal energy}}{\frac{1}{2} \times \text{noise power density}} \end{aligned} \tag{21}$$

By definition, the instantaneous signal power at the filter output is proportional to the square of the output signal, g(t), in the absence of noise. Considering the time, T_d, when g(t) is desired to be a maximum, the signal energy is given by

$$g^2(T_d) = \left(\int_0^{T_d} s(T_d - \tau) h(\tau) d\tau \right)^2 \tag{22}$$

provided that T_d is equal to or greater than the signal duration. Here τ is a time delay variable used as a dummy variable for time in the integration.

According to Parseval's theorem[8], the normalised noise power at the filter output can be expressed as

$$\begin{aligned} P_N &= \frac{N_0}{2} \frac{1}{2\pi} \int_{-\infty}^{\infty} |H(\omega)|^2 d\omega \\ &\equiv \frac{N_0}{2} \int_0^{\infty} h^2(\tau) d\tau \end{aligned} \tag{23}$$

where N_0 is the one-sided noise power spectral density[9] at the filter input, and the function of time h is the Matched filter impulse response function.

From equation (21), the ratio to be maximised is

---

[8] Consider two generic functions of time, $q_1(t)$ and $q_2(t)$, which have Fourier transforms of $Q_1(\omega)$ and $Q_2(\omega)$ respectively. The general form of Parseval's theorem [26] is

$$\int q_1(t) q_2^*(t) dt = \frac{1}{2\pi} \int Q_1(\omega) Q_2^*(\omega) d\omega \; ; \quad d\omega = \frac{2\pi}{dt} \tag{F 4.1}$$

[9] For a continuous function, $h_c(t)$, consider the power contained in the frequency interval between f and f + df. It is usual to regard f as varying from 0 to +∞, making no distinction between positive and negative frequencies. In this case, the one-sided power spectral density [27] of the function is defined as

$$P(f) = |H_c(f)|^2 + |H_c(-f)|^2 \qquad 0 \le f \le \infty \tag{F 4.2}$$

so that the total power is the integral of P(f) from f = 0 to f = ∞. If the function $h_c(t)$ is real, then the two terms are equal, so that $P(f) = 2|H_c(f)|^2$. Occasionally, power spectral densities are defined without this factor of two (called two-sided power spectral densities).

$$\mathrm{SNR} = \frac{g^2(T_d)}{P_N} = \frac{\left[\int_0^{T_d} s(T_d - \tau)h(\tau)d\tau\right]^2}{\frac{N_0}{2}\int_0^{\infty} h^2(\tau)d\tau} \tag{24}$$

Using Schwarz's inequality[10], it can be shown that

$$\mathrm{SNR} \le \frac{\int_0^{\infty} s^2(T_d - \tau)d\tau \int_0^{\infty} h^2(\tau)d\tau}{\frac{N_0}{2}\int_0^{\infty} h^2(\tau)d\tau} \tag{25}$$

which is a maximum when

$$h(t) = k_n s(T_d - t) \tag{26}$$

This is simply the inverse Fourier transform of equation (19), the definition of the matched filter. In general terms, the impulse response of the matched filter is the time-reversed signal function.

The maximum SNR can be expressed as

$$\mathrm{SNR}_{max} = \frac{\int_0^{T_d} s^2(T_d - \tau)d\tau}{\frac{N_0}{2}} \tag{27}$$

The numerator in equation (27) represents the total energy of the signal. Therefore, it can be concluded that the detection capability of a particular signal depends only on its energy content, and not on the time structure.

If the Gaussian noise interference is not white, but can be described by the power spectral density, $|N(\omega)|^2$, then equation (20) becomes

---

[10] One form of Schwarz's [26] inequality states

$$\left(\int_{-\infty}^{\infty} f(x)g(x)dx\right)^2 \le \int_{-\infty}^{\infty} f^2(x)dx \int_{-\infty}^{\infty} g^2(x)dx \tag{F 4.3}$$

$$P_N = \frac{1}{2}\frac{1}{2\pi}\int_{-\infty}^{\infty}\left|N(\omega)H(\omega)\right|^2 d\omega \tag{28}$$

which yields the general optimisation of H(ω), described by

$$H(\omega) = \frac{k_n S^*(\omega)\exp(-j\omega T_d)}{\left|N(\omega)\right|^2} \tag{29}$$

In this application, the target region can give rise to a large amount of clutter. In effect, the sediment volume is composed of many randomly-distributed, independent, broadband scatterers spaced much closer than the resolution capability of the matched filter. Therefore, by virtue of the central limit theorem [28], the clutter signal should resemble a stationary Gaussian random process [29] as a result of the overlap of the many individual signals that are present.

The filter that optimises the signal-to-noise ratio for the general, non-flat spectrum case is given by [26]:

$$H(\omega)_{opt} = \frac{S^*(\omega)}{\frac{N_0}{2} + K_c\left|S(\omega)\right|^2} \tag{30}$$

where $K_c|S(\omega)|^2$ is the clutter power spectrum [30]. If clutter dominates then equation (30) becomes the inverse filter and if noise dominates it becomes the matched filter. (To prevent noise and clutter energy from dominating the filter output, some band-limiting must also be applied.)

Having determined the optimal filter for an arbitrary waveform, it is necessary to find the waveform that best suits the application. In principle, the optimal filter concept can be applied to any waveform. However, certain waveforms give rise to less ambiguous measurements. In this application, high resolution and accuracy are required, *i.e.*, the waveform should leave the least amount of ambiguity to contend with after the filtering process. Earlier in this report, it was suggested that the linear-swept FM chirp is a good choice if a high power and wide bandwidth are required (see section 2.1).

As explained in Appendix A, given a complex time/frequency response function $\chi(\tau,\phi)$, the ambiguity function, $\chi(\tau,\phi)\chi^*(\tau,\phi)$, is used as a criterion that is applied to

the design and analysis of matched filter waveforms. It is used to quantify how well a particular waveform can determine either the velocity and range of a single object, or resolve velocity and range between several objects [31]. (In this investigation, of course, velocity is not an issue.) The ambiguity function is of central importance in the design of matched filter waveforms. A derivation and investigation of its properties is presented in detail in appendix A.

4.3.2 Experimental Measurements

Both matched and inverse filters were used in this investigation. The estimates of the input signal appearing in the filters, $S(\omega)$, were adjusted to include the path-length-dependent attenuation measured in the sediment (see section 2.2.4 of the second report in this series[2]) and the frequency response of the measurement system. It should be noted that these effects could also have been accounted for by adjusting the spectrum of the transmitted pulses (see sections 2.2 and 3.2). In the final analysis whichever method maximises the signal-to-noise ratio, and makes the best use of the dynamic range of the transducers, should be chosen.

The scattering responses of the targets were also included in the filter functions by further modifying the numerator term of equation (30), the general formulation of the optimal filter[11]. This was a target dependent processing method, as discussed in section 2.3, using both the resonant and rigid scattering responses of spherical and cylindrical targets (as discussed in section 3.1).

After optimal filtering, the output signals were squared and time windowed, according to the method described in section 4.1, in a similar way to the scattered power measurements. The peak value in the time window was recorded as the detection result. (It should be noted that it is also common to integrate the squared and time windowed output in optimal filtering applications, or to perform some other kind of envelope detection to locate the signal peak [32].)

---

[11] It should be noted that scattering responses of the targets were not incorporated into the clutter estimate, appearing in the denominator term of equation (30). This is because clutter in the returned signal arises from the interaction between the transmitted signal and the propagation medium. It does not arise from the interaction between the transmitted signal and the target.

In order for this method to be effective, the output waveform had to be suitable for pulse compression processing. The waveform used in this instance was a linear-swept FM pulse, discussed briefly in section 2.1 and in appendix A. It was designed in the time-domain and extended over the entire operational bandwidth of the transducers (sweeping upwards in frequency from 20 kHz to 150 kHz).

As introduced in section 4.2, the abrupt truncation of signals in the time-domain can cause their frequency spectra to become unacceptably distorted unless appropriate windowing functions are used. For the output pulse considered in this case, a $^{1}/_{10}$ cosine-tapered window was chosen as being the most appropriate. The resulting waveform is shown in figure 10.

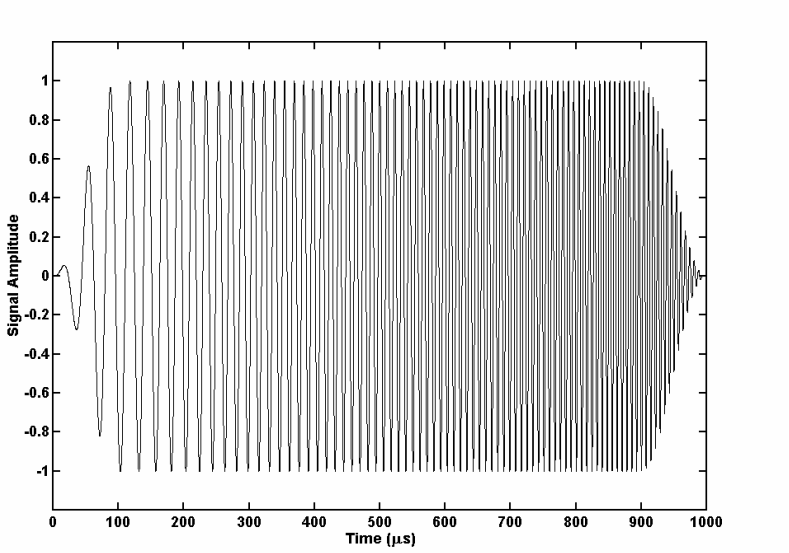

Figure 10 *The time windowed, linear-swept FM (chirp) pulse waveform.*

As before, the buried targets were a steel sphere, a steel cylinder, a polyethylene cylinder and a real cable. Measurements were performed in a similar way to those described in section 3.2. The peak-squared optimal filter output was calculated from every sample point for each different buried object. The results, presented in figures 11 to 26, are also in a similar format to those presented in section 3.2.

The signal-to-noise ratio was calculated so that a comparison could be performed between the different sets of results. It was calculated using a similar method to that described in section 4.2. That is to say, the SNR for each set of measurements was found by dividing the peak value by an estimate of the rms noise level. (Values of SNR in decibels are noted alongside each of the graphs).

The average[12] signal-to-noise ratio for the matched filter measurements is in the range 23.6 - 24.3 dB (figures 11 to 14). However, the peak signal levels in some of the results (such as figure 12, the polyethylene cylinder) correspond to clutter rather than to the target. Therefore, the SNR values obtained from these measurements must be treated with some caution when being compared with other results.

The average SNR for the inverse filter measurements is less than for the matched filter, having a value in the range 21.1 - 22.6 dB (figures 15 to 18). However, there is a marked reduction in the level of clutter in the output plots and, significantly, a higher proportion of the sample points in the target region indicate the presence of a buried object than was the case for the matched filter. Therefore, the inverse filter is judged to be better suited to the detection of buried objects in a cluttered environment.

For the inverse filter, optimised to the elastic scattering response of the targets, the average SNR is in the range 20.0 - 22.3 dB (figures 19 to 22). This overlaps the average SNR of the basic inverse filter (figures 15 to 18). Therefore, these results do not show any quantitative improvement in the use of this filter instead of the basic inverse filter. However, the filter output in the region of the buried targets is, qualitatively, more distinct than in the previous case.

For the inverse filter, optimised to the rigid scattering response of the targets, the average SNR value is in the range 20.9 - 23.4 dB (figures 23 to 26). As in the elastic-scattering-optimised case, this overlaps the average SNR of the basic inverse filter (figures 15 to 18). That is to say, neither of the optimised filters show a quantitative improvement in SNR. However, the target localisation is better than that obtained using the basic inverse filter in both cases.

[12] In this report, the quoted 'averages' of series of decibel values were obtained as follows: Firstly, each decibel value was converted into a linear system of units. The average and the standard deviation of these values were then calculated, to give a range of values with an uncertainty of $\pm$ 1 standard deviation centred on the mean. Finally, this linear result was converted back into the logarithmic (decibel) system of units, to give a range of values that encompassed an estimate of uncertainty.

Original in colour

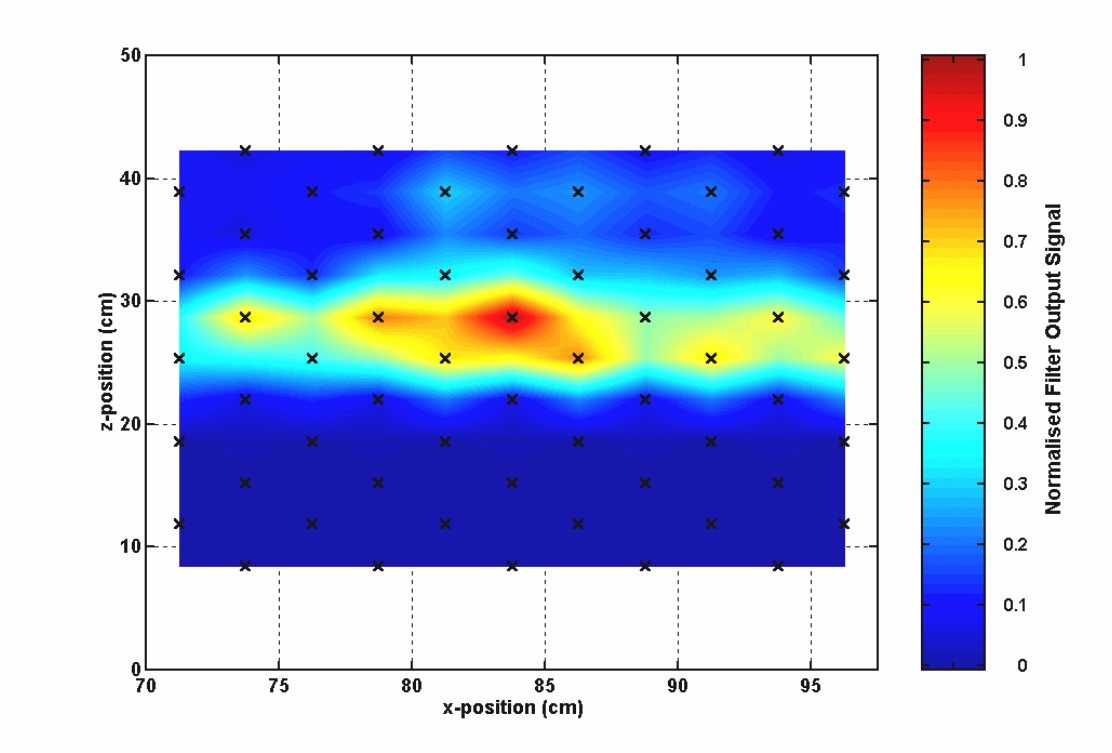

Figure 11 *The normalised, peak-squared, matched filter output from a target region containing a steel sphere (SNR = 24.3 dB).*

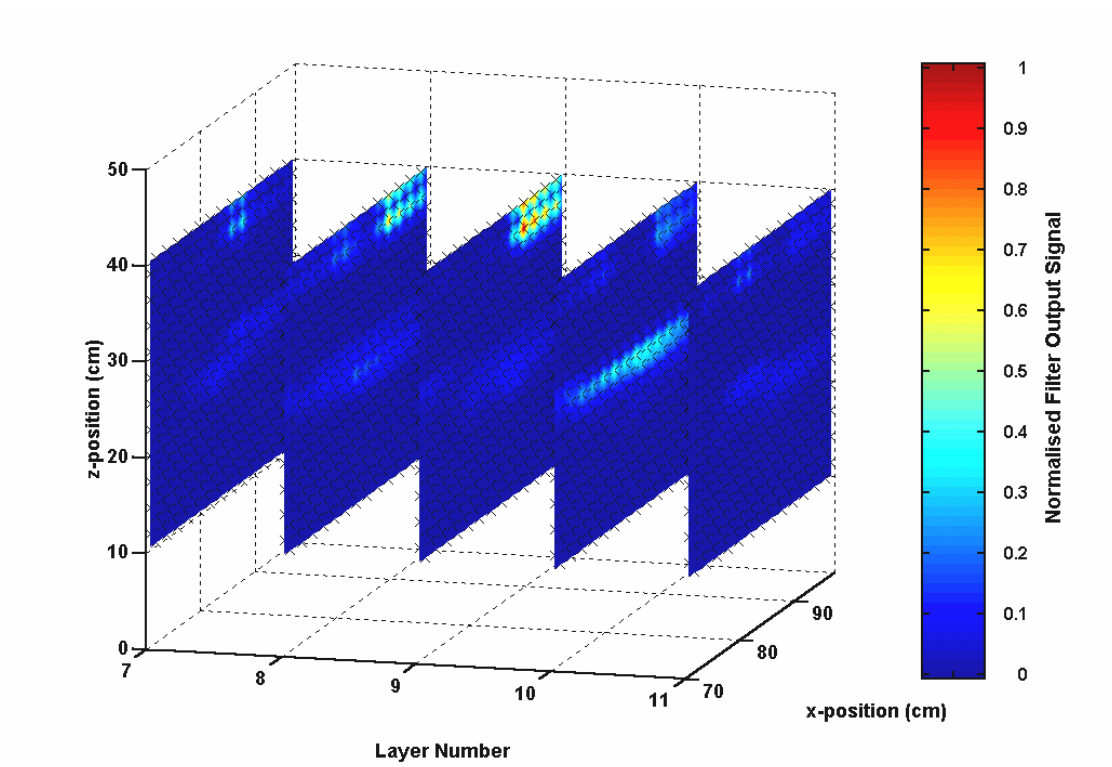

Figure 12 *The normalised, peak-squared, matched filter output from a target region containing a polyethylene cylinder (SNR = 23.4 dB).*

Original in colour

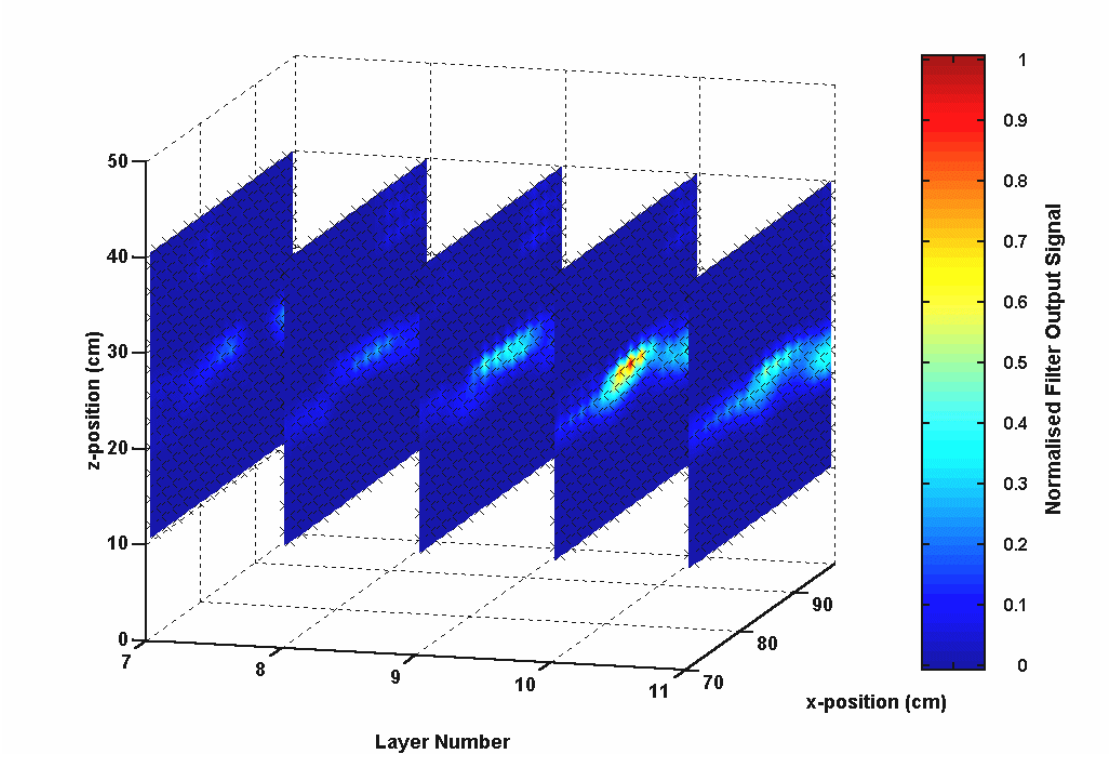

Figure 13 *The normalised, peak-squared, matched filter output from a target region containing a steel cylinder (SNR = 24.0 dB).*

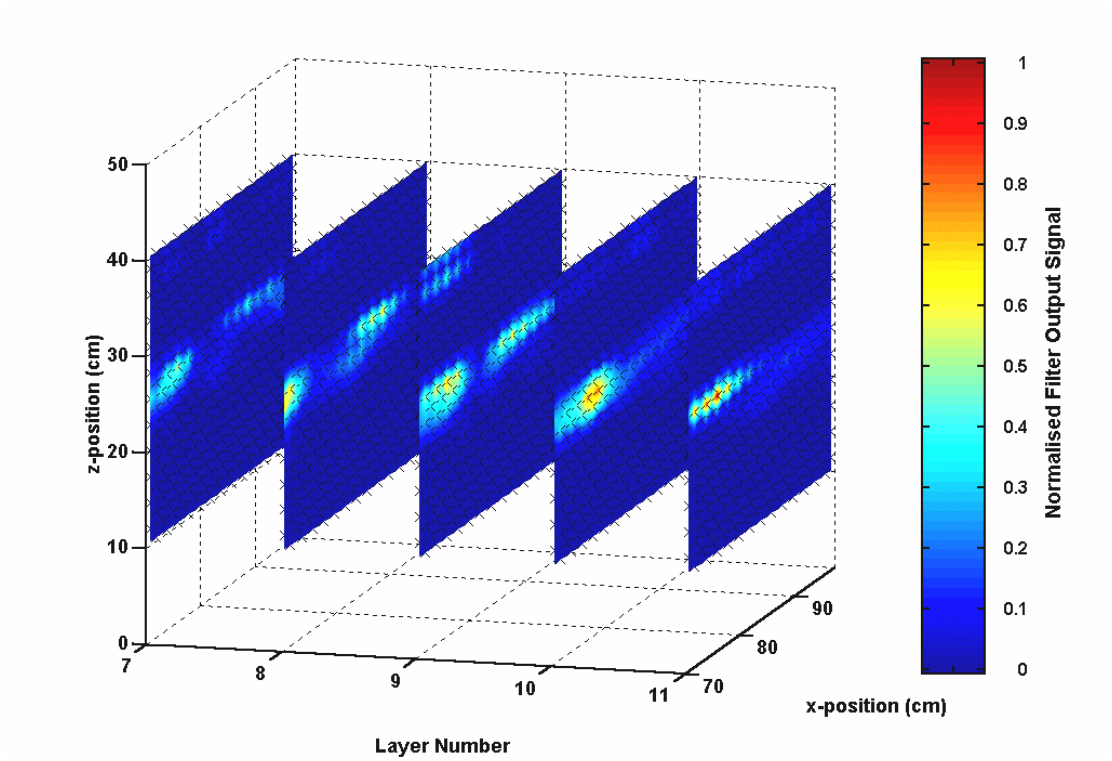

Figure 14 *The normalised, peak-squared, matched filter output from a target region containing a real cable (SNR = 24.1 dB).*

Original in colour

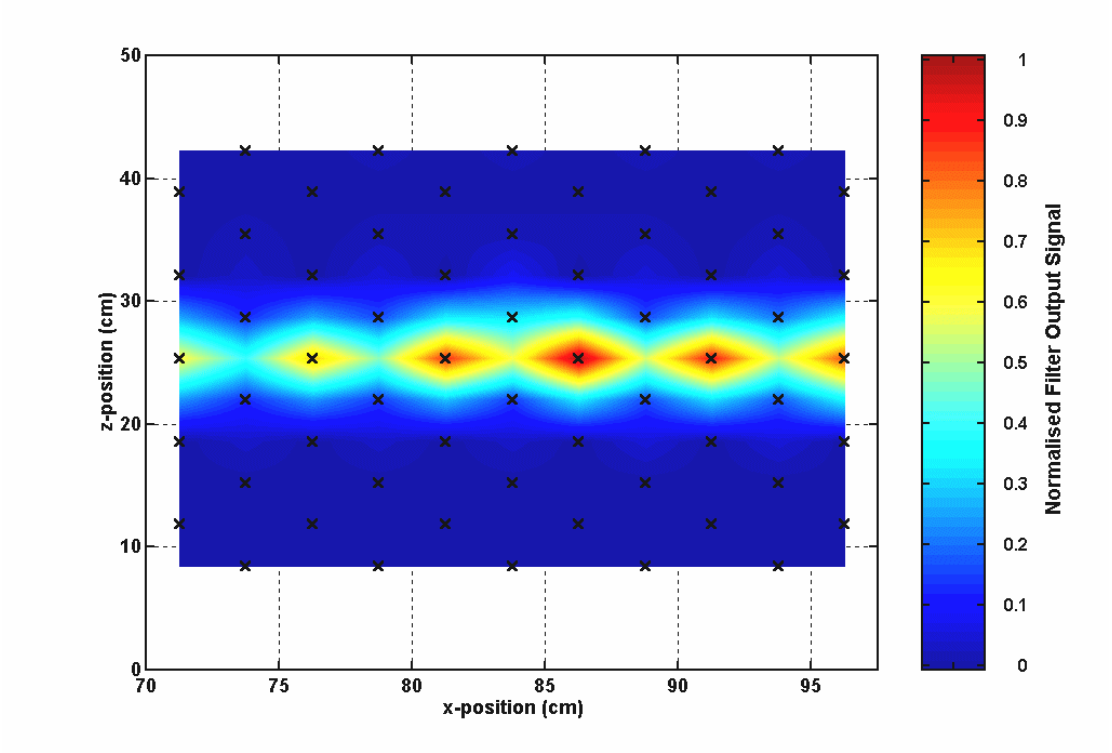

Figure 15 *The normalised, peak-squared, inverse filter output from a target region containing a steel sphere. (SNR = 22.3 dB.)*

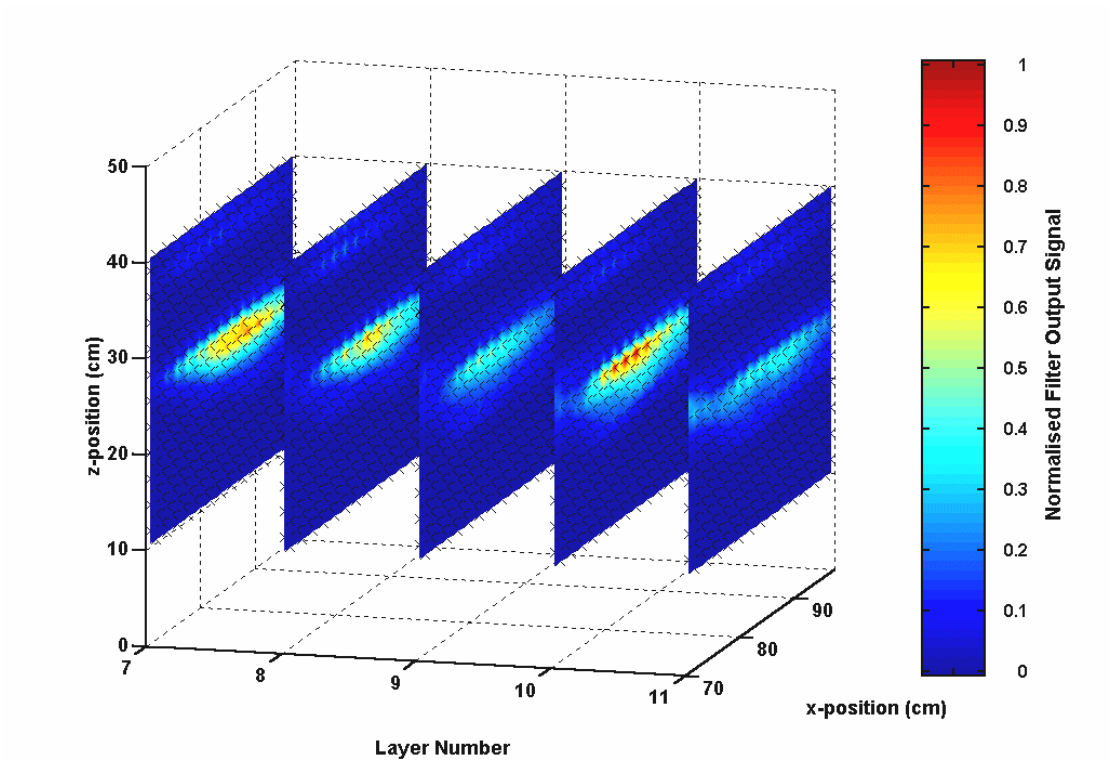

Figure 16 *The normalised, peak-squared, inverse filter output from a target region containing a polyethylene cylinder (SNR = 21.4 dB).*

Original in colour

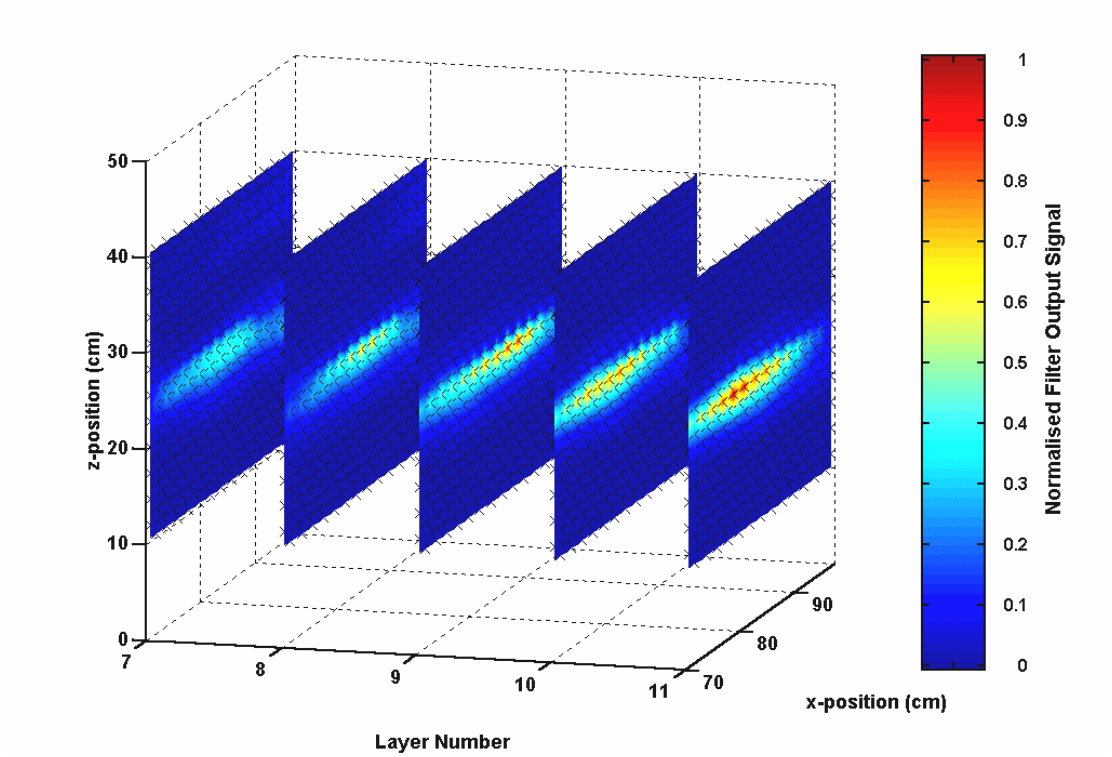

Figure 17 *The normalised, peak-squared, inverse filter output from a target region containing a steel cylinder (SNR = 21.1 dB).*

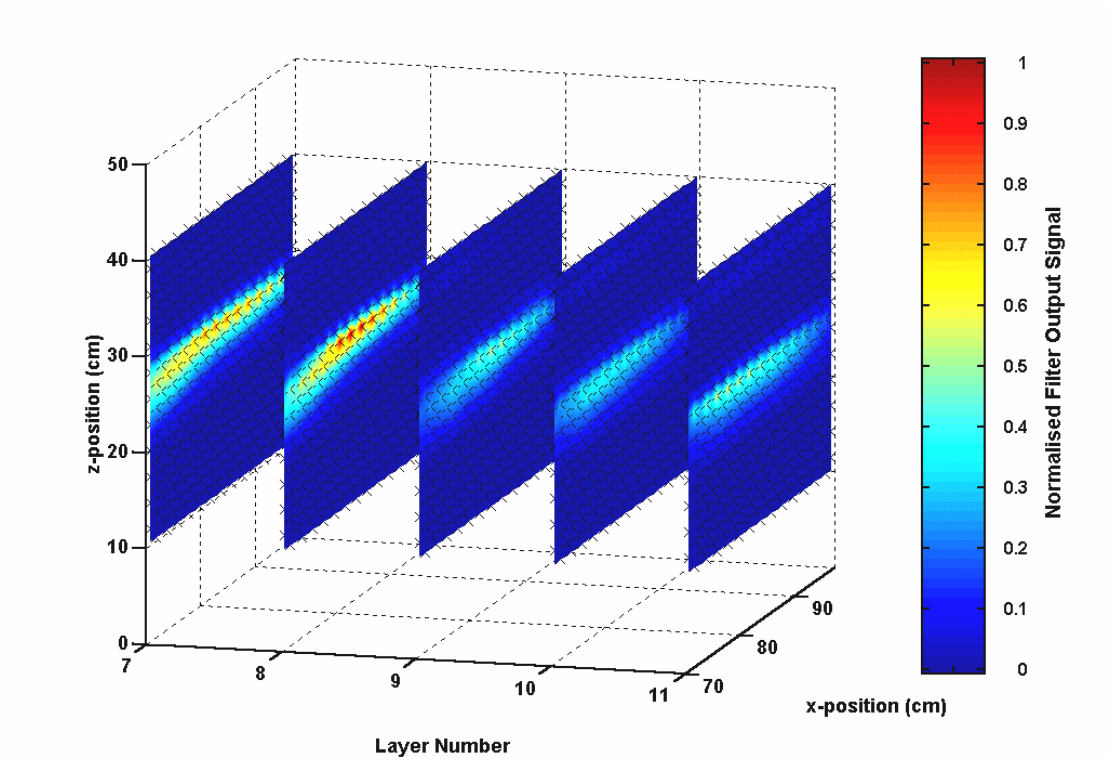

Figure 18 *The normalised, peak-squared, inverse filter output from a target region containing a real cable (SNR = 22.7 dB).*

Original in colour

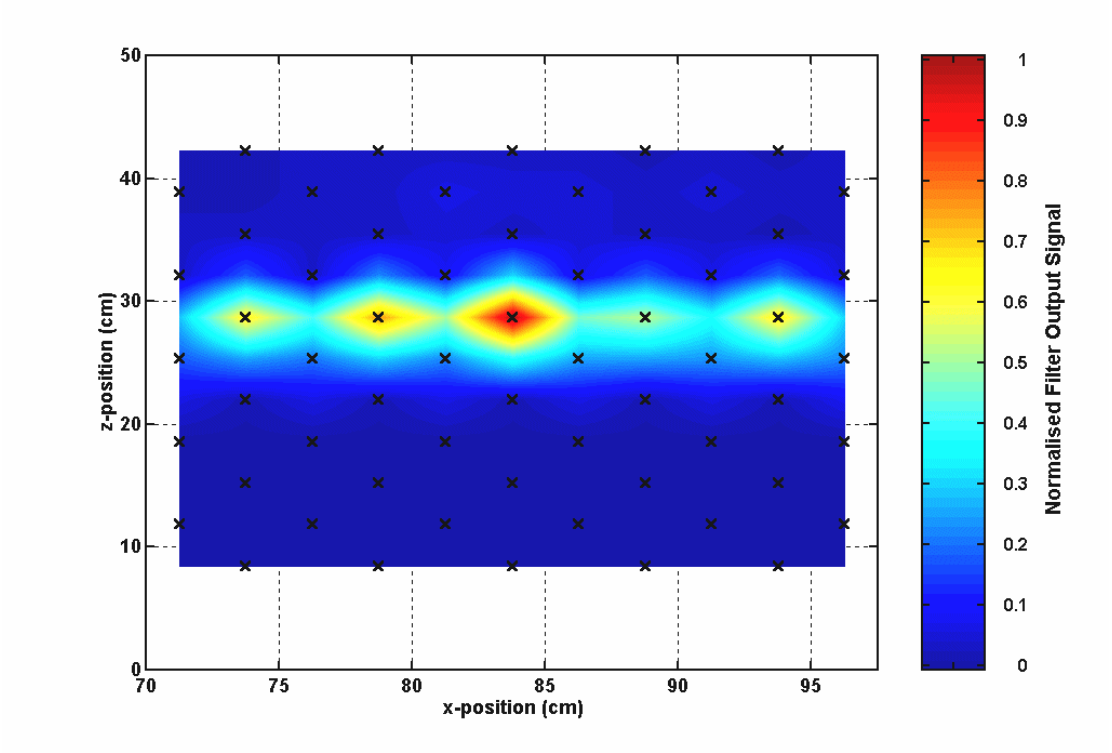

Figure 19 *The normalised, peak-squared, elastic-response-optimised, inverse filter output from a target region containing a steel sphere (SNR = 22.7 dB).*

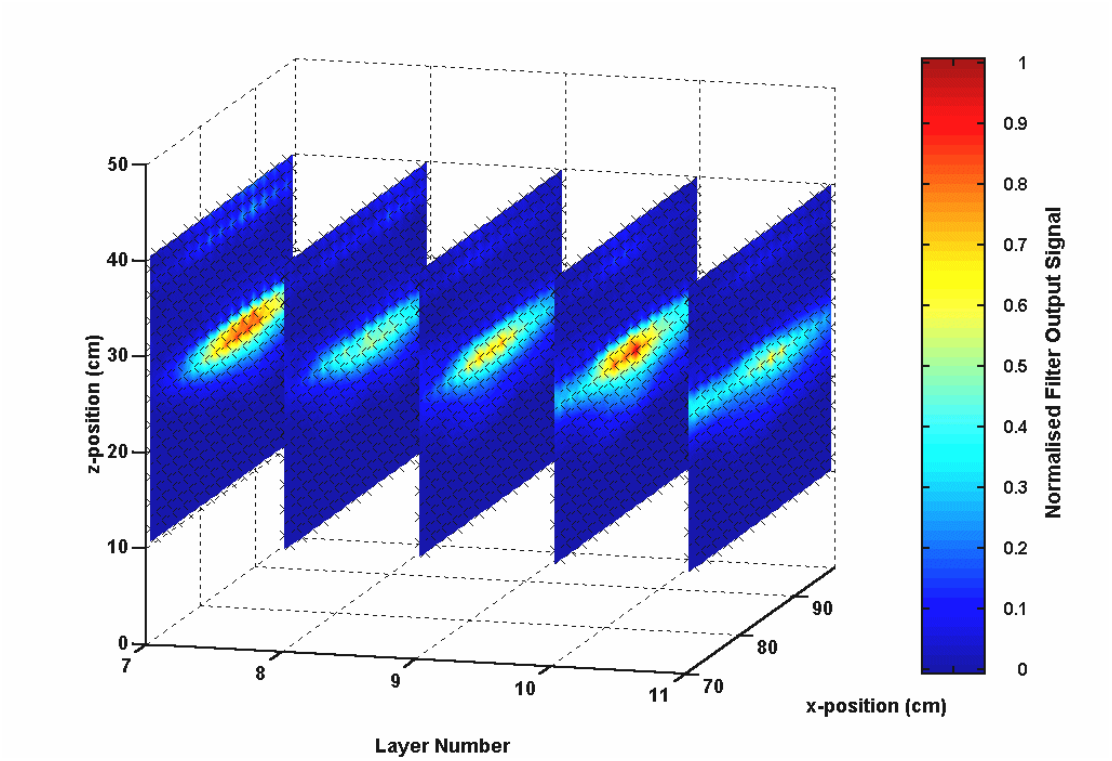

Figure 20 *The normalised, peak-squared, elastic-response-optimised, inverse filter output from a target region containing a polyethylene cylinder (SNR = 20.3 dB).*

Original in colour

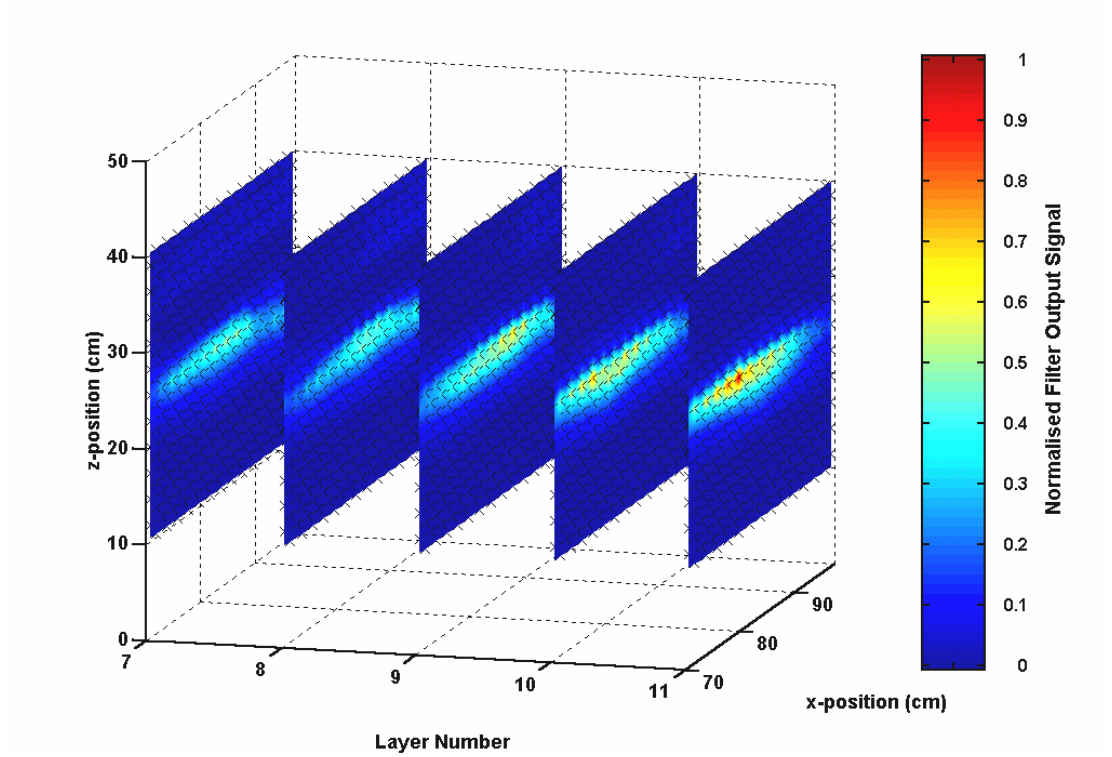

Figure 21 *The normalised, peak-squared, elastic-response-optimised, inverse filter output from a target region containing a steel cylinder (SNR = 21.0 dB).*

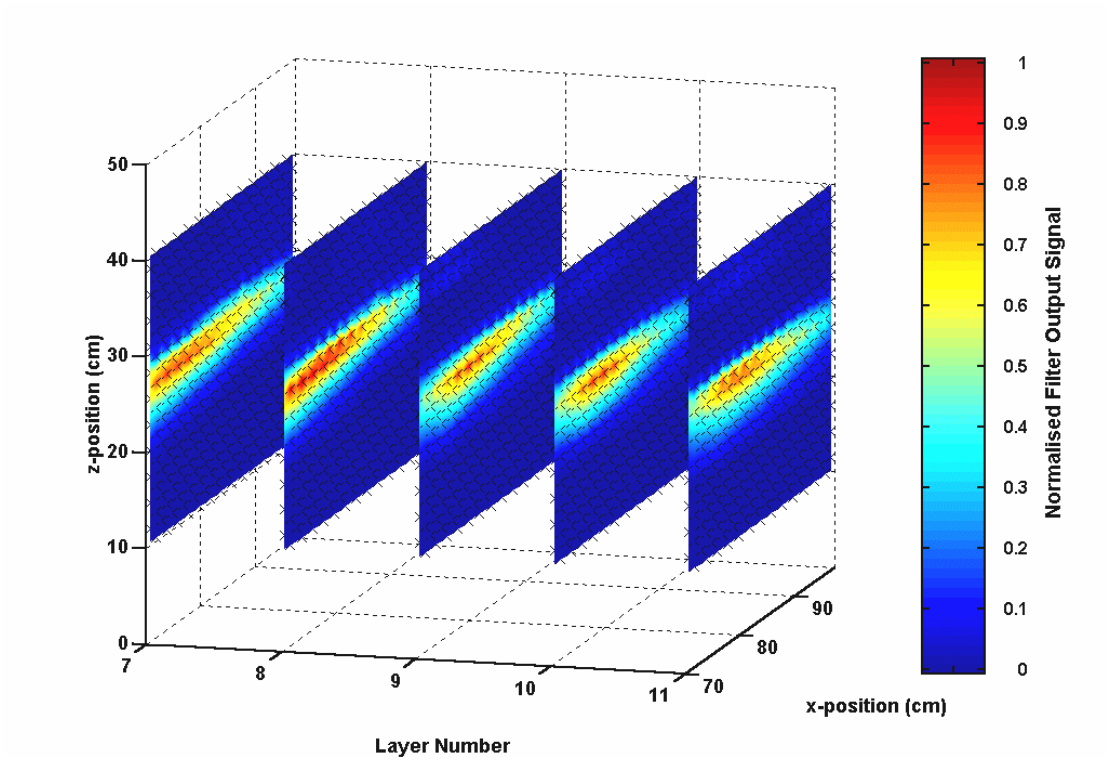

Figure 22 *The normalised, peak-squared, elastic-response-optimised, inverse filter output from a target region containing a real cable (SNR = 20.9 dB).*

Original in colour

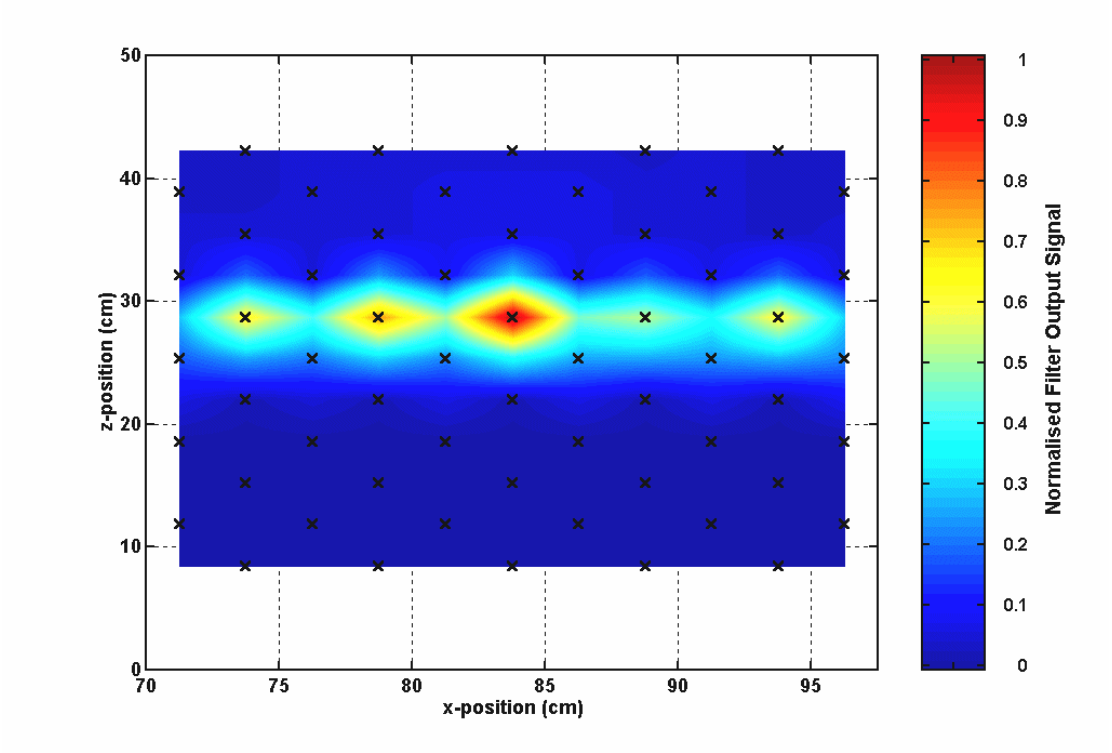

Figure 23 *The normalised, peak-squared, rigid-response-optimised, inverse filter output from a target region containing a steel sphere (SNR = 23.8 dB).*

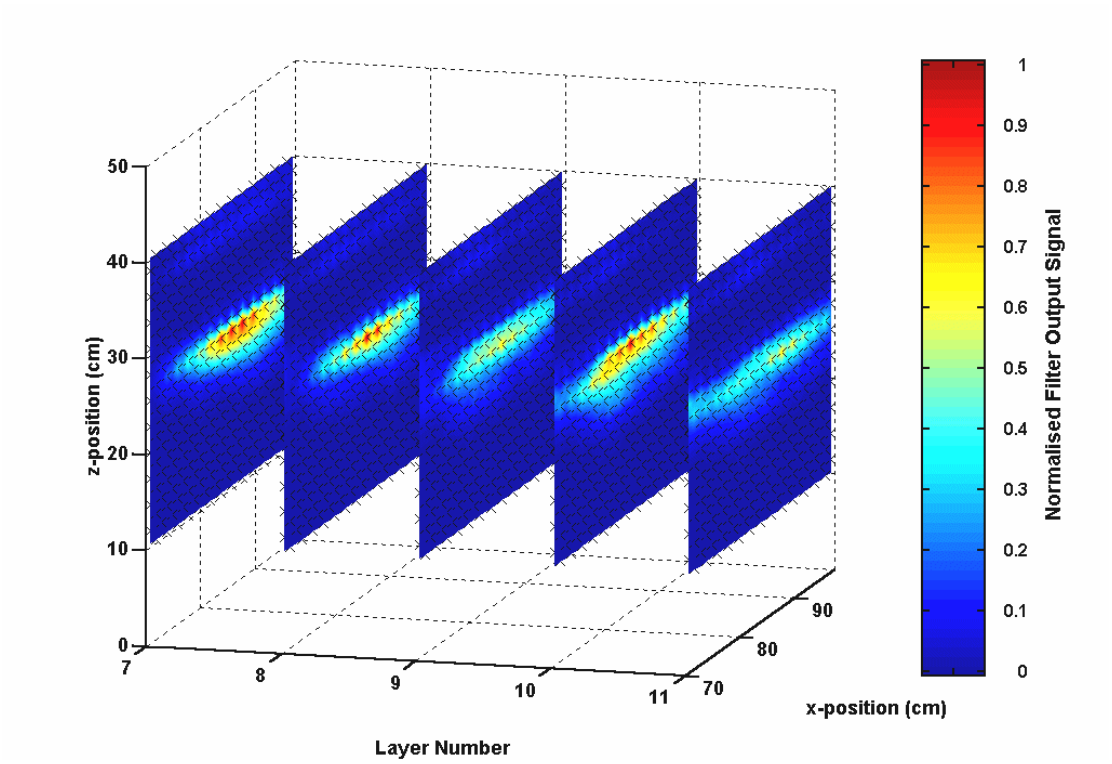

Figure 24 *The normalised, peak-squared, rigid-response-optimised, inverse filter output from a target region containing a polyethylene cylinder (SNR = 21.6 dB).*

Original in colour

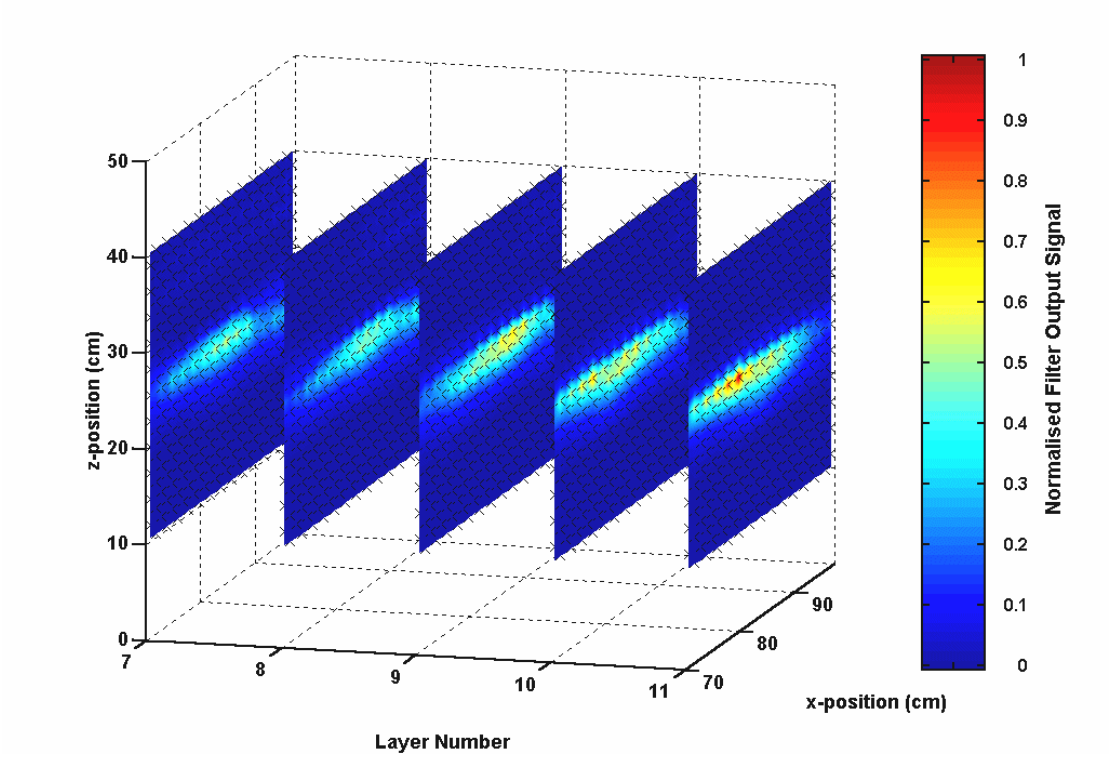

Figure 25 *The normalised, peak-squared, rigid-response-optimised, inverse filter output from a target region containing a steel cylinder (SNR = 21.4 dB).*

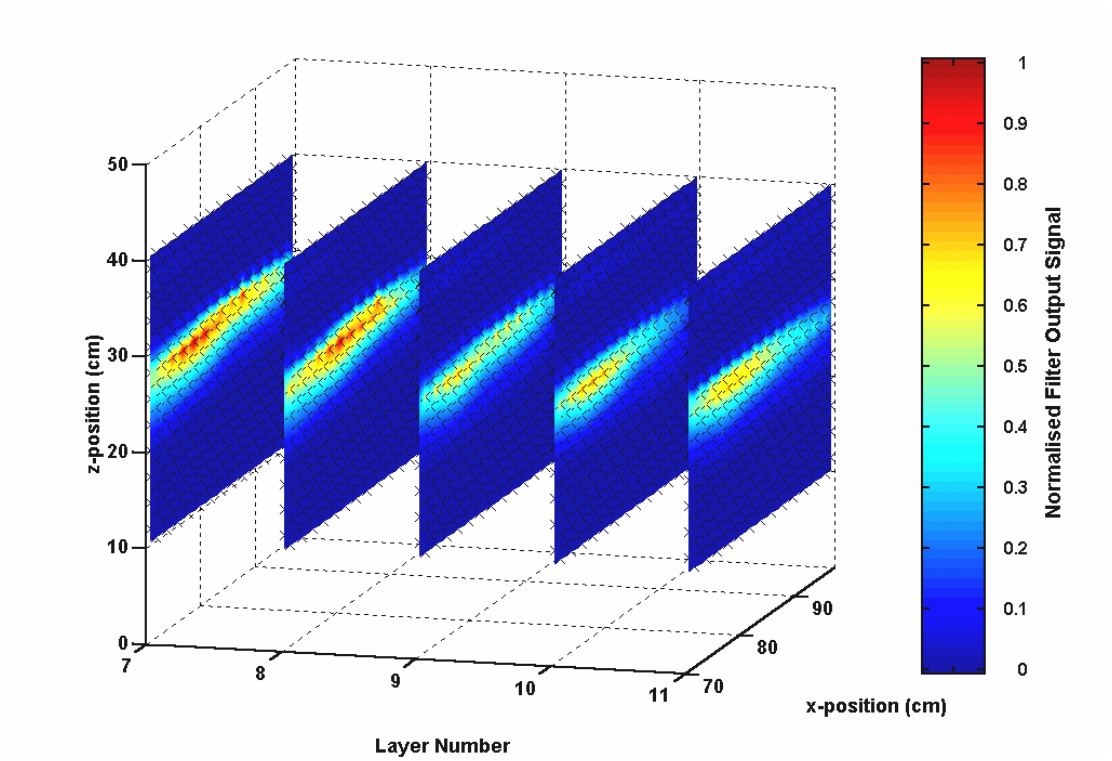

Figure 26 *The normalised, peak-squared, rigid-response-optimised, inverse filter output from a target region containing a real cable (SNR = 21.9 dB).*

4.4 Synthetic aperture techniques

One method of increasing the signal level is to use an array of acoustic sources and receivers [34]. The acoustic signal in the region of the target is then the sum of the signals transmitted from all the sources. Similarly, the measured signal is the coherent sum of the acoustic signals at the array of receivers. This is discussed in section 3 of the second report in this series[2] as a means of achieving a focused, high power acoustic beam.

Similarly, the illusion of an array can be created with a single source / receiver by combining data taken from several different positions in the water. The range covered by the source / receiver is known as the 'synthetic aperture' [35]. An image is formed from a coherent sum of the pings that comprise the aperture. This technique originated in the field of radar and is now well-established as a means of achieving extremely high resolution images. Satellite-borne synthetic aperture radar (SAR) systems have a spatial resolution that is, typically, of the order of 20 - 30 m with a swath width of 100 km [36]. When applied to underwater acoustic systems, this technique is known as synthetic aperture sonar (SAS) [37].

Synthetic aperture systems can be categorised as being either focused or unfocused. A phase variation exists across the aperture due to the relative motion between the sensor and the target, and due to fluctuations in the refractive index of the propagation medium (which are caused by variations in temperature, pressure and salinity). In unfocused systems the two-way phase variation is not removed. In this case, the phase variation must not exceed 90° or else the synthetic aperture data cannot be summed coherently [38]. This condition can be ensured in the laboratory where the path lengths are short and the positions of the transducers can be accurately controlled. In the field, however, it is much more difficult to achieve the performance required. Focused systems seek to overcome this difficulty by tracking the phase variation over the aperture. This results in uniform along-track resolution, independent of both range and frequency [38].

Focused synthetic aperture sonars require some form of navigation system, such as an inertial motion detector, to measure changes in attitude and position. However, to achieve a resolution of the order of centimetres it eventually becomes necessary to

correct the data itself. 'Auto-focus' algorithms can be employed to significantly reduce the effects of residual phase errors that remain after motion compensation. The term, auto-focus, arises from methods in which the estimated platform track is perturbed until the best focus is obtained. Images are then formed by correlating the collected pings with a filter matched to an expected, point-target return [37, 39].

Synthetic aperture sonar is limited by the speed of the detection platform and the pulse repetition frequency (PRF) of the transmitted acoustic pulse. If the target is a long distance from the transducers, the PRF must be kept relatively low to prevent range ambiguities. The along-track resolution is proportional to the distance between measurement points. Therefore, a low PRF and a high platform speed results in poor resolution [38, 40].

It would seem that SAS is well-suited to the current investigation, where the distance from the detection platform to the target is only a few metres, and the platform speed is 'slow' (see section 2.3 of the first report in the series[1]). An issue remains, however, regarding the stability[13] of the transmission medium. Phase coherence studies at various frequencies have shown that seawater is sufficiently stable for synthetic aperture generation [38, 40]. Conversely, the sediment is a complex medium, having both a rough interface and containing volume inhomogeneities that can scatter acoustic energy. The water-sediment interface is examined in detail in the third report in this series[3], where it is concluded that roughness scattering can seriously degrade the performance of a detection system. Such degradation could seriously affect the use of SAS in such an environment.

4.4.1 Experimental Measurements

The data presented in section 4.3 was reprocessed following the synthetic aperture paradigm. For each sample point, a synthetic aperture was formed from the recorded signals corresponding to the point itself and to the nearest four surrounding points. The signals were phase-adjusted to match the signal corresponding to the central point, using the time-of-flight equation (equation 14). Then the average value over the

[13] 'Stability' refers to the variations in the refractive index of the transmission medium over the propagation path. In this case, refractive index changes result from small-scale changes in the temperature and salinity of seawater.

five points was calculated. The resulting signal was processed using the basic inverse filter and a time window was applied to the filter output (according to the method described in section 4.1). The results are shown in figures 27 to 30.

Each of the figures presented below is similar in composition to those presented in sections 4.2 and 4.3. The *z*-direction corresponds to vertical position in the sediment, measured upwards from the bottom of the laboratory tank, and the *x*-direction corresponds to horizontal position. The signal-to-noise ratio was calculated using a similar method to that described in section 4.2. (Values of SNR are noted alongside each of the graphs).

In the synthetic aperture case, the average[14] SNR is 20.9 - 22.4 dB. When compared with the basic inverse filter, which exhibited an average SNR of 21.1 - 22.6 dB (figures 15 to 18), the synthetic-aperture-enhanced filter does not seem to yield any improvement in performance. Moreover, it should be noted that the high signal regions in figures 27 to 30 are not as well localised as before. The apparent lack of improvement using the enhanced technique may be attributed to the fact that only a small number of points were used to create the synthesised aperture. Further investigation using a larger synthetic aperture is required before any conclusions may be drawn as to whether this technique offers any significant improvement.

[14] Refer to footnote 11.

Original in colour

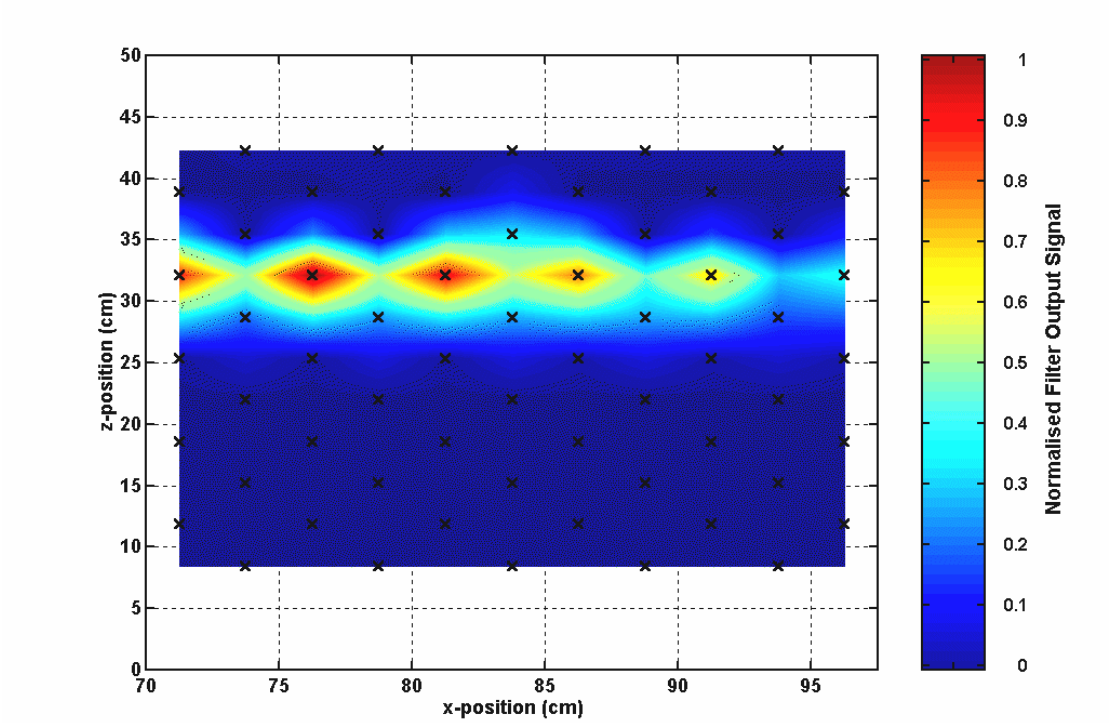

Figure 27 *The synthetic-aperture-enhanced, inverse filter output from a target region containing a steel sphere (SNR = 22.2 dB).*

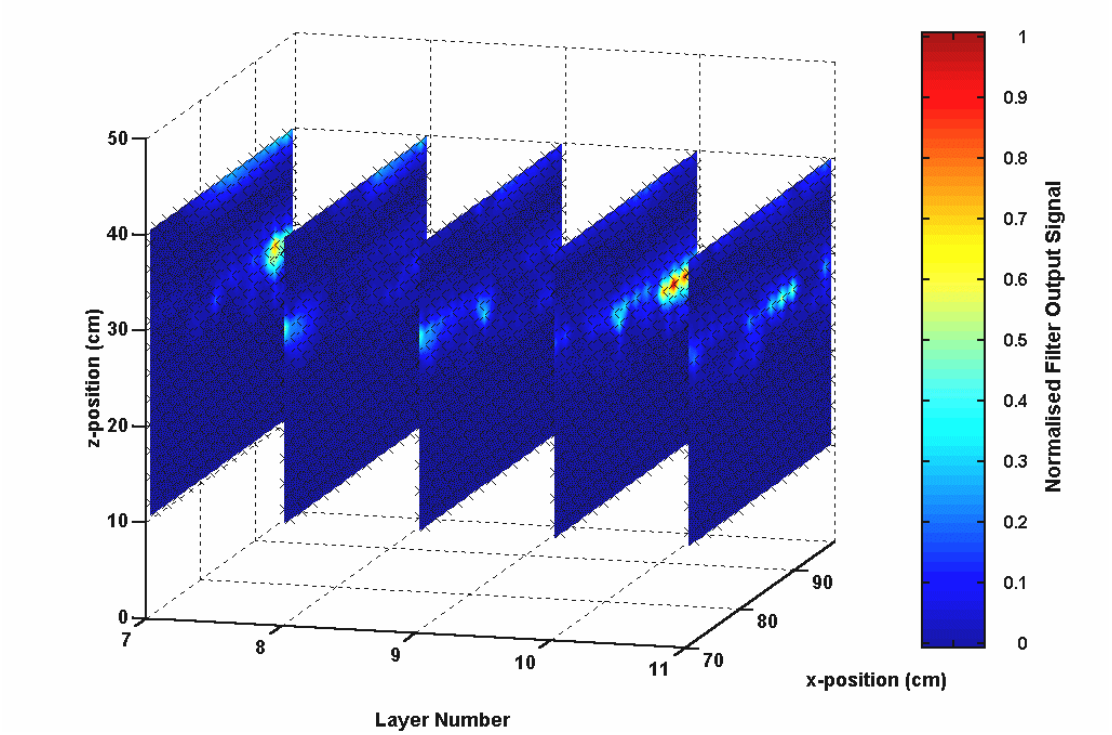

Figure 28 *The synthetic-aperture-enhanced, inverse filter output from a target region containing a polyethylene cylinder (SNR = 21.1 dB).*

Original in colour

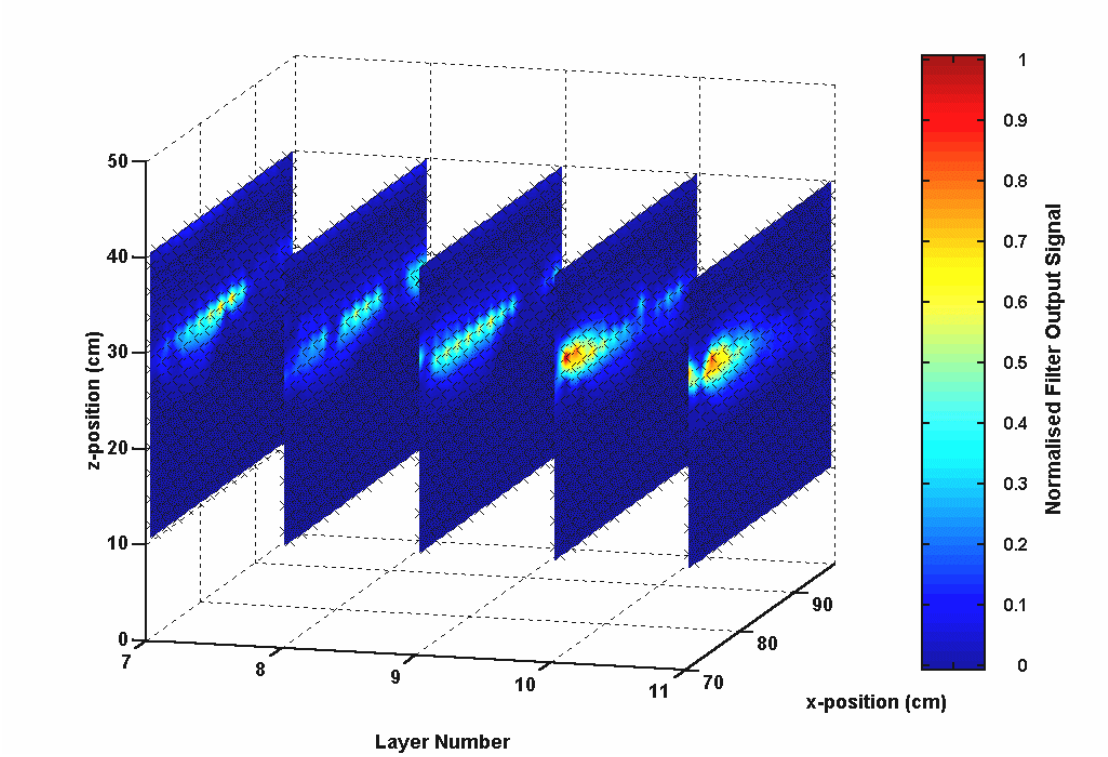

Figure 29 *The synthetic-aperture-enhanced, inverse filter output from a target region containing a steel cylinder (SNR = 21.0 dB).*

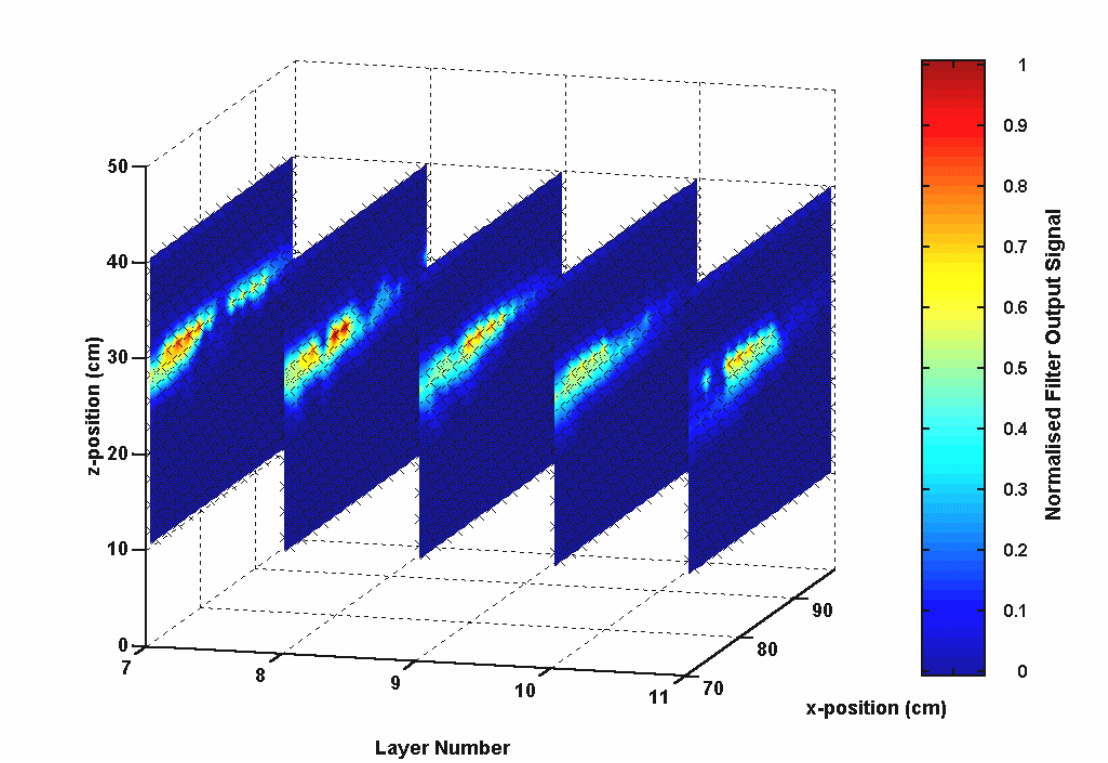

Figure 30 *The synthetic-aperture-enhanced, inverse filter output from a target region containing a real cable (SNR = 22.5 dB).*

4.5 Comparison of Techniques

A comparison of the buried object detection techniques presented in the previous sections is given below. For each technique and buried target type, the signal-to-noise ratio at the output of the processor was recorded. These are summarised in table 2.

Detection Process (Section Number)	Steel Sphere	Polyethylene Cylinder	Steel Cylinder	Real Cable	Average SNR[15]
Scattered Power (4.2)	(18.9)	(19.1*)	(19.5)	(19.9*)	(18.9) – (19.8)
Matched Filter (4.3)	24.3	23.4*	24.0	24.1	23.6 - 24.3
Inverse Filter (4.3)	22.3	21.4	21.1	22.7	21.1 - 22.6
Elastic-Response-Optimised Inverse Filter (4.3)	22.7	20.3	21.0	20.9	20.0 - 22.3
Rigid-Response-Optimised Inverse Filter (4.3)	23.8	21.6	21.4	21.9	20.9 - 23.4
Synthetic-Aperture-Enhanced Inverse Filter (4.4)	22.2	21.1	21.0	22.5	20.9 - 22.4

Table 2 *The signal-to-noise ratios (expressed in dB) that have been calculated for each detection process and target type. An asterisk indicates that the peak signal may correspond to clutter rather than to the target. Note that the scattered power data (shown shaded) are shown for summary purposes only, and should not be compared against the other data in table 2, because they were acquired using a different waveform. Hence they are shown bracketed and shaded.*

It should be noted that in some cases, where the peak clutter levels were comparable to the peak target signals, the SNR estimate may actually be more representative of

[15] Refer to footnote 12.

the peak clutter-to-noise ratio. The measurements for which this may be the case have been marked in the table by an asterisk. Note also that the scattered power data are shown for summary purposes only, and should not be compared against the other data in table 2, because they were acquired using a different waveform. Hence they are shown bracketed and shaded.

Whilst Matched filtering resulted in good SNRs, the associated clutter level was still high, and indeed for the polyethylene cylinder the SNR reflects clutter. Target localisation was unremarkable. Conversely, inverse filtering resulted in lower SNRs than the matched filter. However, from the output plots it is clear that the clutter level was significantly reduced and target localisation greatly improved.

Target optimisation resulted in better localisation of the buried objects in the output images. However, this was not accompanied by an increase in the overall SNR. Given that the resonant scattering response in sediments was not expected to be the same as the theoretical response (for which it was assumed that the surrounding medium was a fluid), it is not entirely surprising that this was the case.

For the rigid scattering inverse filter with synthesised aperture enhancement, the average SNR is in the range 20.9 - 22.4 dB. This level is similar to the average SNR for the basic inverse filter, which was found to be in the range 21.1 - 22.6 dB. However, localisation in the target regions was found to be poor. This is symptomatic of the synthesised aperture process which requires the returned signals to be aligned to within a fraction of a wavelength (typically less than $^1/_5$ of a wavelength). It was concluded that further investigation into the use of this technique is required.

Although not presented in detail here (since the environment that is of interest in this study is highly cluttered) matched filter measurements optimised to resonant and rigid targets have shown similar results to the inverse filter case. It is surmised that the matched filter would be a better choice than the inverse filter for use in a noisy environment, this being consistent with the filter behaviour predicted in section 4.3.

5 Summary

The acoustic detection system hardware has been described in the second report in this series[2]. The aim of this current report was to review the signal processing

requirements of the system and to investigate the relative performance of a number of different detection algorithms.

In order to do this, some basic signal processing concepts were presented and a number of different approaches to detection processing were discussed. It was noted that the detection system should be optimised to the class of object being sought. To this end, the scattering characteristics of spheres and cylinders were calculated. These were used to aid in the selection of an optimal frequency range and were later incorporated directly into the detection algorithms.

In section 4, after preliminary rudimentary tests of the system using a simple scattered power measurement with pulsed AM waveforms, comparative target detection tests were undertaken. Waveform dependent filtering was investigated, using FM pulse compression waveforms.

Overall, the algorithms presented in this report (and the acoustic detection system in general) have proven to be very successful in detecting objects buried at depths of between 25 and 30 cm in the sediment.

In every case, either 60 or 300 sample points were measured over a series of planes extending vertically into the sediment. It was found that with 60 points (having a sample spacing of 5 cm) the resolution was not high enough to provide conclusive detection results. Conversely, with 300 points (having a sample spacing of around 2 cm) the buried objects could be detected quite easily. In a practical system, where the time available for scanning a volume of the seabed may be quite limited, the sample spacing may be adjusted within this range to find the lowest resolution that still provides acceptable performance.

Simple matched filtering was shown to be useful in an environment dominated by noise. However, the optimal filter was shown to be more successful in dealing with the cluttered seabed environment. This is particularly important in light of the findings in the third report in this series[3], where it is noted that surface roughness will give rise to an increase in clutter at the receiver.

Target optimisation techniques had mixed success. When the target scattering responses (for both rigid and the elastic scattering) were incorporated into the filters,

qualitative improvements in target localisation were observed. However, these were not accompanied by an increase in the average values of the signal-to-noise ratio.

Synthetic aperture techniques have also been investigated. It was suggested that these may have the potential to improve the performance of a detection system. However, the positional error in the laboratory apparatus and the small number of measurement positions used to form the synthetic aperture meant that no significant performance improvement was actually observed.

This material formed the basis of the PhD of RCPE [41-44].

APPENDIX A

FM WAVEFORM DESIGN

A.1 Complex Waveform Representation

Let $\psi(t)$ be a complex time domain waveform, the real part of which is the driving signal $s_{real}(t)$, and let $\Psi(\omega)$ be the complex frequency-domain representation of $\psi(t)$.

Consider the class of real waveforms that can be described by

$$s_{real}(t) = a(t)\cos[2\pi f_0 t] + \theta(t) \tag{A 1}$$

where a(t) is an envelope function, $\theta(t)$ is the phase modulation and f_0 is the carrier frequency. For analysis involving linear operations on $s_{real}(t)$, it is convenient to use [45]

$$s_{real}(t) = \mathrm{Re}\{\psi(t)\} \tag{A 2}$$

where $\psi(t)$ is a complex waveform that has a real part equal to $s_{real}(t)$. In general, the analysis can be accomplished in less steps using the complex representation and invoking the real operator, $\mathrm{Re}\{\ldots\}$, after having completed all the linear operations.

A more convenient form of $\psi(t)$ for linear systems analysis is given by the Gabor representation [46]:

$$\psi(t) = s_{real}(t) + j\frac{1}{\pi}\int_{-\infty}^{\infty}\frac{s(\tau)}{t-\tau}d\tau \tag{A 3}$$

The real part consists of $s_{real}(t)$, as required, and the imaginary part is the Hilbert transform of $s_{real}(t)$. It can be difficult to derive this waveform since it is usually not possible to express the Hilbert transform in closed form. In practice, therefore, the Gabor representation is often approximated by

$$\psi(t) = u(t)\exp(j2\pi f_0 t) \quad ; \; u(t) = a(t)\exp\left[j\theta(t)\right] \tag{A 4}$$

In general, the imaginary parts of equations (A 3) and (A 4) will not be equal. For the remainder of this appendix, all waveforms will be treated in terms of this complex representation.

A.2 The Ambiguity Function

The ambiguity function is a measure of the difference between a waveform, $s_{real}(t)$, and its time and frequency shifted self, *i.e.*, it is a measure of how accurately the range and velocity of a target can be estimated and of how reliably two targets can be resolved [47]. Ambiguity is characterised by a two-dimensional waveform amplitude distribution function in time delay, τ, and frequency displacement, ϕ. The ambiguity function is defined as $\chi(\tau,\phi)\chi^*(\tau,\phi)$, where

$$\chi(\tau,\phi) = \int_{-\infty}^{\infty} u(t)u^*(t+\tau)\exp(-j2\pi\phi t)dt \tag{A 5}$$

is the complex time / frequency response function.

The ambiguity function is derived by considering the mean square difference between s(t), represented by the real part of the complex function $\psi(t)$, and its time and frequency shifted self, $\psi(t + \tau, f + \phi)$. Note that this criterion is only one of many possible measures of the difference between two waveforms but it is considered to be appropriate for this investigation:

$$\int_{-\infty}^{\infty} \left|\psi(t) - \psi(t+\tau, f+\phi)\right|^2 dt = k_1 - 2\cdot \mathrm{Re}\left\{\int_{-\infty}^{\infty} \psi(t)\psi^*(t+\tau, f+\phi)dt\right\} \tag{A 6}$$

where k_1 is a normalisation constant related to the signal energy,

$$k_1 = \int_{-\infty}^{\infty} \left|\psi(t)\right|^2 dt + \int_{-\infty}^{\infty} \left|\psi(t+\tau, f+\phi)\right|^2 dt \tag{A 7}$$

Only the integral on the right hand side of equation (A 6) is significant. This term is the general correlation function for simultaneous shifts in time and frequency. It achieves its maximum value when $\tau = \phi = 0$.

Applying equation (A 4), the relationship between u(t) and ψ(t):

$$\int_{-\infty}^{\infty} \psi(t)\psi^*(t+\tau, f+\phi)dt = \exp\left[-j(f_0+\phi)\tau\right] \times \int_{-\infty}^{\infty} u(t)u^*(t+\tau)\exp(-j2\pi\phi t)dt \quad \text{(A 8)}$$

The integral on the right hand side of equation (A 8) is recognised as $\chi(\tau, \phi)$, previously defined in equation (A 5).

The origin of the integral can be placed anywhere in the plane shown in figure A 1, having co-ordinates of absolute range delay, T_d, and frequency, f_0. The τ - ϕ plane can be treated as the time / frequency space in which the sonar signals of interest exist.

It is possible for the correlation function to have peaks at locations away from the origin. The implication is that the ψ(t) functions of the signals which correspond to these peaks are indistinguishable. This makes the estimation of time and frequency ambiguous. In the case where the number of targets is unknown, there is no way of being certain how many are actually being observed.

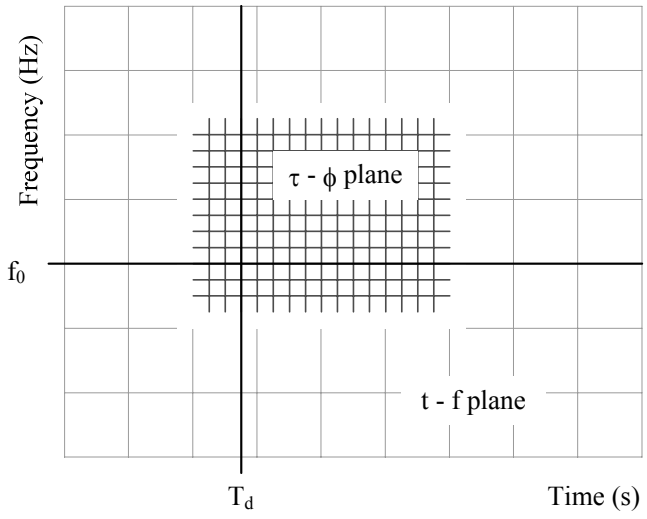

Figure A 1 *The ambiguity function time / frequency co-ordinate plane. The origin,* $\tau = \phi = 0$*, is located at range delay,* T_d*, and frequency,* f_0*.*

A.2.1 The Doppler Approximation

The Doppler effect appears as a scaling factor on the time variable of a waveform reflected from a moving target and results in a time displacement (*i.e.*, a range error) on the compressed pulse at the matched filter output [48]. Consider a point target travelling at constant velocity, v, along a radial path *away* from an acoustic source. If

$\psi(t)$ is transmitted then the reflected waveform is $\psi(t - t_d)$, where the delay time, t_d, is a function of time:

$$t_d = \frac{2R(t)}{c_w} \quad \text{and} \quad R(t) = R_0 - vt \tag{A 9}$$

where c_w is the speed of sound in the water and R_0 is the range of the target at time, $t = 0$. By substituting for t_d and collecting terms, the result obtained is

$$\psi(t - t_d) = \psi\left(\alpha t - \frac{2R_0}{c_w}\right) \quad \text{where} \quad \alpha = 1 + \frac{2v}{c_w} \tag{A 10}$$

and $2R_0/c_w$ is the nominal range delay to and from the target. Similarly, by changing the sign in the equations the Doppler-shifted waveform can be found for a target travelling along a radial path *towards* an acoustic source.

An important Fourier transform pair is

$$\psi(\alpha t) \Leftrightarrow \Psi(f/\alpha) \tag{A 11}$$

where $\Psi(\omega)$ is the complex frequency-domain representation of $\psi(t)$ (as stated earlier).

This implies that the correct matched filter for a Doppler-shifted waveform has the form $\Psi^*(f/\alpha)$ and not the usually implemented $\Psi^*(f \pm \phi)$. However, as long as the time-bandwidth product of a Doppler-shifted signal is less than $c_w/2v$, the matched filter response can be treated using $\Psi^*(f \pm \phi)$.

A.2.2 The Time Resolution Constant

A quantitative basis for judging the potential resolution of a waveform in situations which do not involve a Doppler shift, is the 'time resolution constant' [49]:

$$T_R(0) = \frac{\int_{-\infty}^{\infty} |\chi(\tau,0)|^2 \, d\tau}{|\chi(0,0)|^2} \tag{A 12}$$

where χ is the ambiguity function, as in equation (A 5), and τ is a time delay variable. It is reasonable to assume that, in most cases, the waveform that gives the smallest value for $T_R(0)$ has the greatest potential for resolving between two signals in time.

For equal energy waveforms that have a fixed bandwidth, the time resolution constant achieves its smallest value when the frequency band is fully occupied. This leads to an important conclusion: When it is known that there will be no Doppler shift, single pulse transmissions are less ambiguous than a train of pulses. Also, $T_R(0)$ will be smallest when the spectrum has a uniform height. In this case, the linear FM pulse approximates the optimum band limited waveform for resolving between several signals as long as they do not suffer any significant frequency displacement.

The associated 'frequency resolution constant' [49], which gives the resolution between two signals as a function of frequency with no significant time delay, is given by

$$F_R(0) = \frac{\int_{-\infty}^{\infty} \left|\chi(0,\phi)\right|^2 d\phi}{\left|\chi(0,0)\right|^2} \tag{A 13}$$

where ϕ is a frequency delay. A measure of the combined resolving capability of a waveform is given by the product $T_R(0)F_R(0)$. For a single tone Gaussian windowed pulse, $T_R(0)F_R(0) = 1$, and for a single tone rectangular windowed pulse, $T_R(0)F_R(0) = {}^2/_3$. Therefore, rectangular pulses appear better suited to situations requiring a combined time delay / Doppler shift resolving capability.

Finally, the time resolution constant including variations in frequency (*i.e.*, Doppler shift), $T_R(\phi)$, and the frequency resolution constant including variations in time delay, $F_R(\tau)$, are given by [49]

$$T_R(\phi) = \frac{\int_{-\infty}^{\infty} \left|\chi(\tau,\phi)\right|^2 d\tau}{\left|\chi(0,0)\right|^2} \quad ; \; F_R(\tau) = \frac{\int_{-\infty}^{\infty} \left|\chi(\tau,\phi)\right|^2 d\phi}{\left|\chi(0,0)\right|^2} \tag{A 14}$$

A.3 FM Pulse Compression Waveforms

The most significant property of the ambiguity function is that the total potential ambiguity, as measured by the volume under the surface generated by the function, is independent of the type of signal employed (as long as all signals are normalised to have the same energy content). Broadly speaking, all signals can be considered to be equally as good. However, each waveform will give a different distribution of ambiguity that will result in one waveform being more appropriate for a particular detection scenario than another.

The ambiguity function provides the basis for a systematic search for the best waveform for a particular application. The procedure that is normally adopted is to examine a range of waveforms and to choose the one that gives the best fit to the desired ambiguity function. The degree to which this can be done is an indication of how well the system will perform in the projected environment.

The 'thumbtack' ambiguity function is the closest realisation of a single impulse ambiguity surface [50]. It consists of a narrow spike at $\tau = \phi = 0$ surrounded by a uniformly low pedestal. There is no waveform that can exactly match the thumbtack although the linear-swept FM pulse is a reasonable approximation in the zero Doppler case. The ambiguity surface for a linear FM pulse, sweeping upwards in frequency over a bandwidth of 100 kHz and having a time duration of 1 ms, is presented in figure A 2.

The ambiguity associated with swept-frequency signals that have undergone a Doppler shift can be reduced by adding non-linearity to the sweep rate, *e.g.*, the hyperbolic FM pulse [51]. However, the drawback with non-linear FM pulses is the increase in the sidelobe response of the matched filter output. If sidelobe energy is relatively large and extends over an appreciable time interval, smaller signals at different range locations can be masked by sidelobes from larger signals. This is of particular importance in multiple scattering environments such as the seabed. The ambiguity surface for a parabolic FM waveform [52], having similar time and bandwidth properties to the linear waveform, is presented in figure A 3.

Original in colour

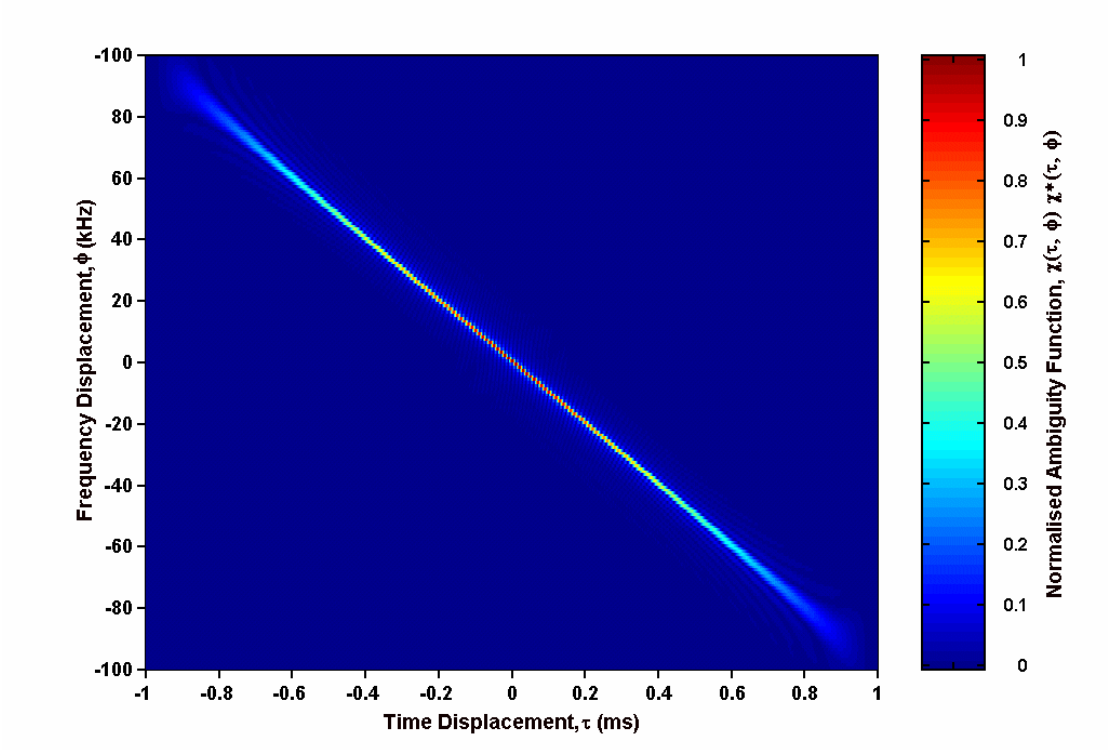

Figure A 2 *The ambiguity surface for a linear FM pulse, sweeping upwards in frequency over a bandwidth of 100 kHz and having a time duration of 1 ms.*

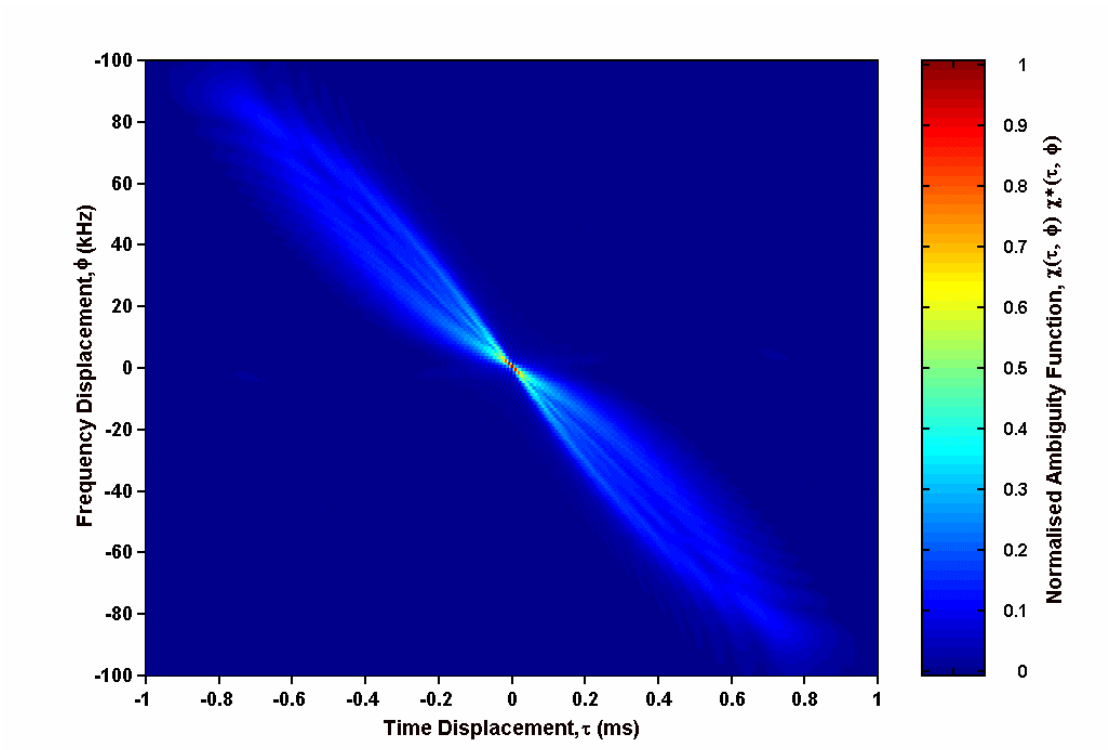

Figure A 3 *The ambiguity surface for a parabolic FM pulse, sweeping upwards in frequency over a bandwidth of 100 kHz and having a time duration of 1 ms.*

References

[1] Daniels D J, Gunton D J, Scott H E, "Introduction to subsurface radar", *IEE Proceedings*, Volume 135, Part F, Number 4, pp. 278 - 320, August 1988.

[2] Daniels D J, "Surface-penetrating radar", *IEE Electronics & Communication Engineering Journal*, Volume 8, Number 4, pp. 165 - 182, April 1996.

[3] *A Dictionary of Physics*, 3rd Edition, Oxford University Press, 1996.

[4] Kock W E, *Radar, Sonar, and Holography. An Introduction*, Academic Press, New York and London, 1973.

[5] Burdic W S, *Radar Signal Analysis*, Prentice-Hall, Inc., London, p. 311, 1968.

[6] Arthur J W, "Modern SAW-based pulse compression systems for radar applications. Part 1: SAW matched filters", *IEE Electronics & Communication Engineering Journal*, Volume 7, Number 6, pp. 236 - 246, December 1995.

[7] Arthur J W, "Modern SAW-based pulse compression systems for radar applications. Part 2: Practical systems", *IEE Electronics & Communication Engineering Journal*, Volume 8, Number 2, pp. 57 - 78, April 1996.

[8] Press W H, Teukolsky S A, Vetterling W T, Flannery B P, *Numerical Recipes in C: The art of scientific computing*, 2nd Edition, Cambridge University Press, Section 13.3, pp. 547 - 549, 1995.

[9] Malecki I, *Physical Foundations of Technical Acoustics*, Chapter 6, Pergamon Press, Oxford, 1969.

[10] Flax L, Gaunard G C, Überall H, "Theory of Resonance Scattering", (Mason W P, Thurston R N, *Physical Acoustics*, Volume XV, Part B, Academic Press, Inc., pp. 191 - 294, 1981).

[11] Numrich S K, Howell W E, Subrahmanyam J V, Überall H, "Acoustic ringing response of the individual resonances of an elastic cylinder", *Journal of the Acoustical Society of America*, Volume 80, Number 4, pp. 1161 - 1169, October 1986.

[12] Hackman R H, "Acoustic Scattering from Elastic Solids", (Pierce A D, Thurston R N, *Physical Acoustics*, Volume XXII, Academic Press, Inc., p. 8, 1993).

[13] Zerr B, Tesei A, Maguer A, Fox W L J, Fawcett J A, "Target Classification Methodology Combining Reconstruction from Multiple Aspects and Resonance Scattering Analysis", *Proceedings of the Fourth European Conference on Underwater Acoustics*, pp. 813 - 818, Edited by A Alippi and G B Cannelli, Rome, 1998.

[14] Maze G, Lecroq F, Decultot D, Ripoche J, Numrich S K, Überall H, "Acoustic scattering from finite cylindrical elastic objects", *Journal of the Acoustical Society of America*, Volume 90, Number 6, pp. 3271 - 3277, December 1991.

[15] Tsui C Y, Reid G N, Gaunard G C, "Resonance scattering by elastic cylinders and their experimental verification", *Journal of the Acoustical Society of America*, Volume 80, Number 2, pp. 382 - 389, August 1986.

[16] Abramowitz M, Stegun I A, *Handbook of Mathematical Functions*, Dover Publications, Inc., New York, 1972.

[17] Hickling R, "Analysis of Echoes from a Solid Elastic Sphere in Water", *Journal of the Acoustical Society of America*, Volume 34, Number 10, pp. 1582 - 1592, October 1962.

[18] Urick R J, *Principles of Underwater Sound*, Third Edition, McGraw-Hill Book Company, p. 319, 1983.

[19] Kinsler L E, Frey A R, Coppens A B, Sanders J V, *Fundamentals of Acoustics*, Third Edition, John Wiley & Sons, p. 419, 1982.

[20] Burdic W S, *Underwater Acoustic System Analysis*, Prentice Hall, Section 10.1, pp. 298 - 302.

[21] Potter J R, Lim T W, Chitre M, "High frequency ambient noise in warm shallow water", *Proceedings of the Fourth International Conference on Natural Physical Processes associated with Sea Surface Sound*, pp. 45 - 54. Edited by T G Leighton, Southampton, 1997.

[22] Nielsen R O, *Sonar Signal Processing*, Artech House, Inc., pp. 97 - 99, 1991.

[23] Urick R J, *Principles of Underwater Sound*, Mc-Graw Hill, New York, 1975.

[24] Nielsen R O, *Sonar Signal Processing*, Artech House, Inc., 1991.

[25] Woodward P M, *Probability and Information Theory, with Applications to Radar*, Pergamon Press, Oxford, 1953.

[26] Cook C E, Bernfeld M, *Radar signals - an introduction to theory and application*, Chapter 2, Academic Press, 1967.

[27] Press W H, Teukolsky S A, Vetterling W T, Flannery B P, *Numerical Recipes in C: The art of scientific computing*, 2nd Edition, Cambridge University Press, p. 498, 1995.

[28] Barlow R J, *Statistics*, John Wiley & Sons, pp. 49 - 50, 1996.

[29] Barlow R J, *Statistics*, John Wiley & Sons, pp. 34 - 41, 1996.

[30] Cook C E, Bernfeld M, *Radar signals - an introduction to theory and application*, Chapter 10, pp. 338 - 341, Academic Press, 1967.

[31] Cook C E, Bernfeld M, *Radar signals - an introduction to theory and application*, Chapter 4 Academic Press, 1967.

[32] Meyer D P, Mayer H A, *Radar Target Detection: Handbook of Theory and Practice*, Academic Press, London, 1973.

[33] Bierens L H J, "Hardware design for modern radar processing", *IEE Electronics & Communication Engineering Journal*, Volume 9, Number 6, pp. 257 - 270, December 1997.

[34] Nielsen R O, *Sonar Signal Processing*, Artech House, Inc., p. 63, 1991.

[35] Daviss B, "Snap happy under the sea", *New Scientist*, pp. 31 - 37, 22June, 1996.

[36] Griffiths H, "Interferometric synthetic aperture radar", *IEE Electronics & Communication Engineering Journal*, Volume 7, Number 6, pp. 247 - 256, December 1995.

[37] Shippey G, Kröling O, "Steps Towards Interferometric SAS Imaging using a Wideband Chirp Source", High Frequency Acoustics in Shallow Water, SACLANTCEN Conference Proceedings CP-45, NATO SACLANT Undersea Research Centre, pp. 483 - 492, 1997.

[38] Bruce M P, “A processing requirement and resolution capability comparison of side-scan and synthetic-aperture sonars”, *IEEE Journal of Oceanic Engineering*, Volume 17, Number 1, pp. 106 - 117, 1992.

[39] Guyonic S, “Effect of waveform on synthetic aperture sonar performances”, High Frequency Acoustics in Shallow Water, SACLANTCEN Conference Proceedings CP-45, NATO SACLANT Undersea Research Centre, pp. 205 - 214, 1997.

[40] Bruce M P, “Correction to 'A processing requirement and resolution capability comparison of side-scan and synthetic aperture sonars' (Jan. 92 106-117)”, *IEEE Journal of Oceanic Engineering*, Vol. 17, No. 2, p. 222, April 1992.

[41] Evans, R C P, “Acoustic penetration of the seabed, with particular application to the detection of non-metallic buried cables”, *PhD Thesis, University of Southampton,* 1999.

[42] Evans R C. Leighton T G, “The Detection of cylindrical objects of low acoustic contrast buried in the seabed”, *J. Acoust. Soc. Am.*, Vol. 103, p. 2902, 1998.

[43] Evans R C,. Leighton T G, “The Detection of Cylindrical Objects of Low Acoustic Contrast Buried in the Seabed”, *Proceedings of the 16th International Congress on Acoustics and 135th Meeting of the Acoustical Society of America (ICA/ASA ‘98)*, Edited by Kuhl P K and Crum L A, pp. 1369 - 1370, 1998.

[44] Evans R C, Leighton T G, “An experimental investigation of acoustic penetration into sandy sediments at sub-critical grazing angles”, *Proceedings of the Fourth European Conference on Underwater Acoustics*, Edited by Alippi A and Cannelli G B, pp. 697 - 702, 1998.

[45] Burdic W S, *Radar Signal Analysis*, Prentice-Hall, Inc., London, p. 149, 1968.

[46] Qian S, Chen D, “Joint Time-Frequency Analysis”, *IEEE Signal Processing Magazine*, pp. 52 - 67, March 1999.

[47] Nielsen R O, *Sonar Signal Processing*, Artech House, Inc., pp. 191 - 193, 1991.

[48] Cook C E, Bernfeld M, *Radar signals: An introduction to theory and application*, Academic Press, p. 64, 1967.

[49] Cook C E, Bernfeld M, *Radar signals - an introduction to theory and application*, Section 4.11, Academic Press, 1967.

[50] Cook C E, Bernfeld M, *Radar signals - an introduction to theory and application*, Section 4.12, Academic Press, 1967.

[51] Nielsen R O, *Sonar Signal Processing*, Artech House, Inc., p. 218, 1991.

[52] Cook C E, Bernfeld M, *Radar signals: An introduction to theory and application*, Academic Press, p. 98, 1967.